Dispersion of virus-laden droplets in ventilated rooms: effect of homemade facemasks

Aliyu M. Aliyu[1*], Dharminder Singh[1,2], Chino Uzoka[1], Rakesh Mishra[1]

[1]School of Computing and Engineering, University of Huddersfield, Queensgate, HD1 3DH, United Kingdom

[2]School of Computing, Engineering and Built Environment, Glasgow Caledonian University, Cowcaddens Road, Glasgow G4 0BA, United Kingdom

Abstract

In December 2019, a new coronavirus (the SARS-CoV-2) emerged and since then it has rapidly spread throughout the world. It causes the respiratory disease called COVID-19. Microbial pathogens of respiratory infectious diseases are often transmitted through particles during speaking, sneezing and coughing. Therefore, understanding the particle movement is important for infection control through mitigating strategies. Computer modelling (using Computational Fluid Dynamics (CFD)) has become a useful tool in studying and visualising the spread of atomised droplets during breathing, coughs and sneezes. In this study, CFD simulations were carried out in a pair of rooms to study the extent of respiratory droplet transfer from one room to the other with and without a facemask. A porous facemask with pore size of 600 µm was used, representing the pore size of a typical homemade facemask. Experts have suggested that such masks may be useful in preventing the transmission of infected respiratory droplets. Velocities of droplets ejected used in the simulations ranged from 5 to 15 m/s for coughs and 10 to 20 m/s for sneezes. Their sizes range between 1 and 2000 µm with a mean size of 32.6 and 17.5 µm for coughs and sneezes respectively and are all based on experimental studies reported in the literature. Using the discrete phase model (DPM), the transport of ejected droplets was studied with and without a facemask. The results show that the facemask trapped more than 90% of all the ejected droplets in both coughing and sneezing scenarios and a further 6-7% are trapped in the recommended 2 m social distancing radius around the human source. Correspondingly, only 60-80% of droplets are deposited within the 2 m radius in the no facemask scenarios, with up to 40% of droplets remaining airborne and transported further to the other room. Based on the CFD data, one-dimensional empirical models were developed for the droplet concentration as a function of the droplet Weber number and the distance from the bioaerosol source. The models show that droplet concentration decays exponentially away from the source especially in cases where facemasks are used. The study therefore reinforces the importance of using face coverings to lessen the transmission of possibly infected respiratory droplets that could transmit highly infectious diseases such as COVID-19.

Keywords: Bio-aerosols**,** Computational fluid dynamics, COVID-19, facemask, isolation rooms, respiratory droplets, ventilation.

1 Introduction

The SARS-Cov2 virus that causes COVID-19 has proven to be highly infectious and its outbreak clearly reveals the risks that respiratory infectious diseases pose to the very connected modern world. Mitigation measures (such as unprecedented travel restrictions, business and school closures, track & trace and quarantine procedures) have been implemented to curtail its spread. The main transmission modes for the transfer of infected aerosolised droplets from host subject to the surroundings is through respiratory and contact routes [1]. These so-called respiratory droplets can be emitted through coughing and sneezing as well as from mere breathing and these droplets have a size of 10 µm or less. These phenomena are responsible for transmitting the virus to a distance of more than 2

m even within indoor spaces. The virus can linger in the air for hours and deposit on surfaces under the normal ventilation conditions provided in hospitals, domestic, and industrial environments. There are several factors that affect droplet dispersion and hence infection transmission. These include room temperature and humidity, air-conditioning, if the windows are open or closed, general air quality, room size and number of people present and their proximity to each other.

While it has been widely suggested that season affects aerosol and hence virus transmission, a UK Government report into SARS-Cov2 transmission [2] noted that the direct influence winter conditions likely have on its spread is insignificant. Winter conditions may increase viral endurance on outdoor surfaces due to reduced temperatures and ultraviolet (UV) radiation levels from the sun. It may also increase viral persistence in unheated indoor environments due to lower temperatures during the winters. Furthermore, outdoors aerosols can persist due to reduced UV levels, however, the risk infection is quite low because of higher ventilation. Hence, the report noted that outdoors, viral transmission is not a major concern, while in indoor environmental conditions, the risk of infection increases primarily because most of the human activity during winter is limited to indoors. Hence there a weak connection between the season and virus survival, and only the secondary effect of human behaviour may contribute to virus transmission indoors. This stance is further buttressed by Lipsitch [3] with data from the summer and autumn of 2009 during the flu pandemic in the United States.

One of the reasons infectious coronaviruses rapidly spread throughout the world is that the mechanisms of respiratory droplets transport along with ambient or ventilated air in indoor spaces are not fully known [4]. Experimental studies have shown that the maximum direct reaches of the particles and microclouds driven by sneezing and coughing are mainly unaffected by indoor environmental airflows [5], but there is increasing evidence the smallest aerosolised particles can be transported for very long distances along with the airflow. Since the outbreak of Covid-19, computer modelling (using CFD) has proven to be a useful tool in studying and visualising the spread of atomised droplets during breathing, coughs and sneezes [6], [7].

Recent studies have attempted to show the spread of discharged aerosolised droplets in various indoor and outdoor scenarios using CFD simulations. These include those which confirmed that 1.5 m is not sufficient for social distancing to prevent immediate deposition of cough droplets on a person but indeed it should be 2 m [8]. Also, simulations found that it is best to not walk or run directly behind others to avoid inhaling droplets in their wake's slipstream [9]. For Indoor environment, medical advice stipulates that suspected coronavirus-infected persons are isolated in separate rooms. Simulations carried out [10] showed that while a patient in the indoor environment wearing a surgical mask significantly mitigates the risk of virus-laden droplets spreading within a room, leakages may still occur. As a result, cohabitants of a house with an isolated patient may still be exposed to airborne secretions. How this occurs is still a subject of ongoing research. The droplet spreading patterns and dispersion mechanisms between rooms, and residence time of droplet in the indoor environment requires more investigation under different scenarios that represent domestic, hospital, commercial, and industrial settings. Ong et al. [11] demonstrated that SARS-Cov2-infected particles were found in ventilation systems in hospital rooms of patients with the disease in China. Bourouiba [12] noted that finding virus particles in ventilation tracks and far areas from the host patient is consistent with the turbulent gas cloud theory of disease transmission as it gives a description of how particles can travel long distances from subjects.

Research [13] has shown that using face masks can reduce infection transmission among the general population. However, due to N95 and other surgical facemasks generally reserved for healthcare workers in many countries around the world during the Covid-19 pandemic, the use of non-surgical

facemasks has been advocated to prevent spread in the general population [14], [15]. In the early days of the pandemic, the United States CDC advised [16] that people should wear cloth facemasks outdoors and the Surgeon General demonstrated how to make a cloth facemask in a few steps [17]. When used properly, such masks have the potential to reduce the spread of the coronavirus from both symptomatic and asymptomatic persons [18]–[21]. However, it has been stated that due to the porous nature of these masks, they only offer a limited degree of protection [13], [22], [23] and must be used together with other interventions such as social distancing. To what extent infectious secretions that leak from such masks, become airborne and spread is still not clear.

In this paper, we present a computational fluid dynamics (CFD) investigation to study the spread of fine droplets (which could be virus-laden) from coughs and sneezes with and without the use of such masks. The aim is to establish the efficacy of a cloth facemask in an indoor space under prevailing ventilation conditions. A typically porous facemask was modelled under coughing and sneezing conditions in a two-roomed building. The geometry of the building used here is based on the model by Kalliomaki and co-workers [24]–[27] which they considered as a representative case for hospital containment rooms. We used the discrete phase model (DPM) to track the trajectories of possibly infected droplet ejecta from coughs and sneezes in order to determine the extent of inter-room transfer. This will improve the understanding of the spreading patterns of potentially virus-laden droplets in well-ventilated rooms.

2 CFD modelling

2.1 Geometry and meshing

The geometry of the indoor environment consists of a two-roomed building, adapted from Kalliomaki et al. [27], was built with Ansys DesignModeler® v19.2. It consists of an inner isolation or source room which is connected to the anteroom by a doorway (of width 1.10 m and height 2.06 m) in the middle of a separating wall (Figure 1 (a)). The length and width of the rooms is 4.7 m and 4.0 m respectively; and their height is 3.0 m. This gives a volume of 56.4 m^3 for each room. Each room has a circular inlet ventilation port located at the middle of the ceiling of the room and a 280 x 180 mm outlet discharge port located 2.62 m from the ground and next to the dividing wall between the rooms.

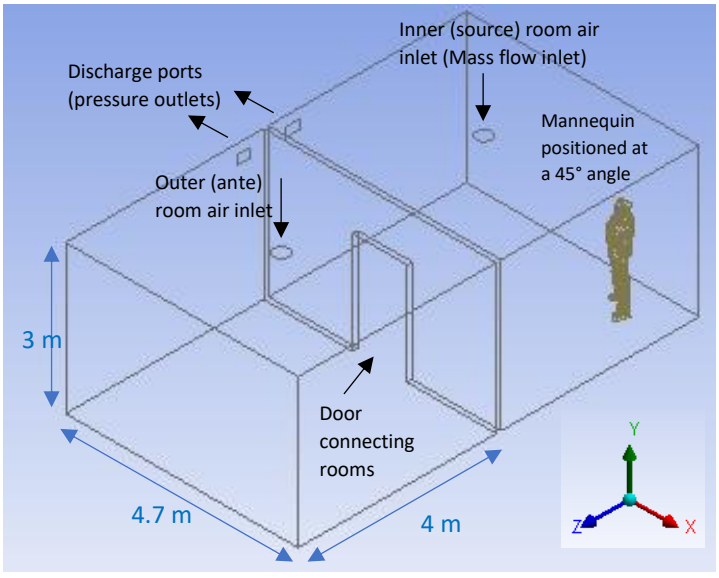

(a)

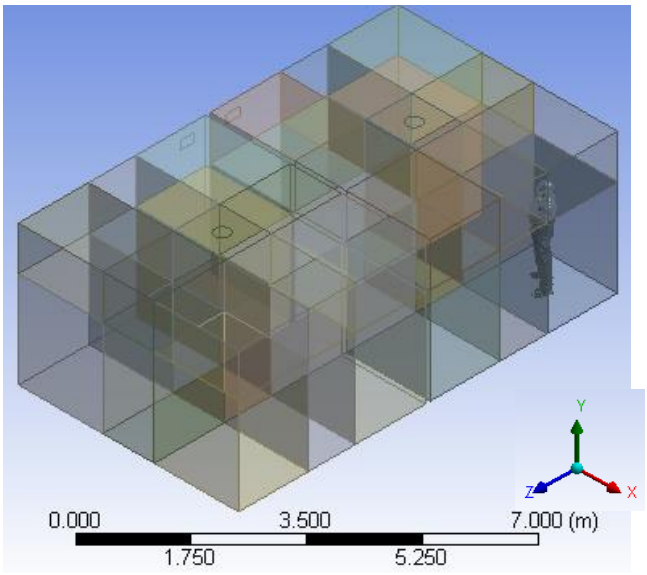

(b)

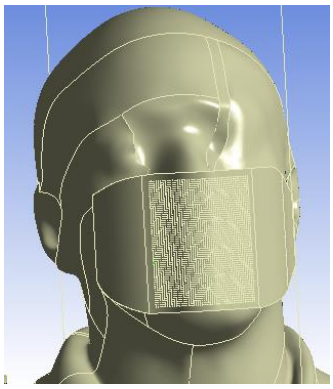

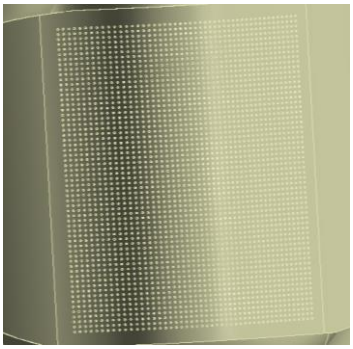

(c) (d)

Figure 1: CAD models showing (a) rooms geometry including locations of inlet/outlet ports and mannequin (b) segmentation of the geometry for selective meshing (c) face mask on mannequin (d) details of face mask pore arrangement with 600 µm pore sizes spaced 1500 µm.

This arrangement of air inlet and outlet ports is known as the top-supply-top-exhaust configuration for hospitals and clinics isolation rooms that produces mixing ventilation [28]–[30]. A mannequin was placed at an oblique angle of 45° facing the door at a far end corner of the inner room, which will serve as a human source of ejected coughs and sneezes. Because of the presence of the mannequin, the non-hexahedral-shaped faces and in order to use an optimal number of mesh elements, each of the rooms was divided into 18 segments (Figure 1 (b)) to allow for selective meshing of each segment using the appropriate mesh element type and size. Two test cases involving the mannequin were considered for the simulations. The first case consists of a mannequin without a facemask fitted, while the second case consists of a mannequin with a facemask fitted. The CAD model of the facemask was created and was designed to have 2,820 holes of 600 µm in diameter with a 1500-µm horizontal and vertical spacing between them (Figure 1 (c) and (d)). The hole size was chosen to be within the midrange of 100 to 1178 µm for woven materials used for cloth facemasks [31].

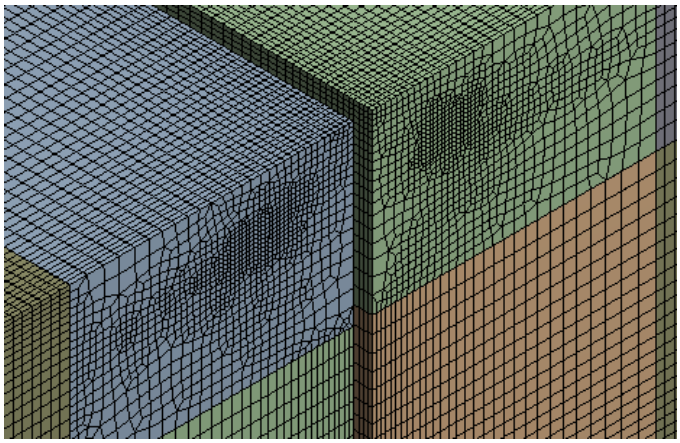

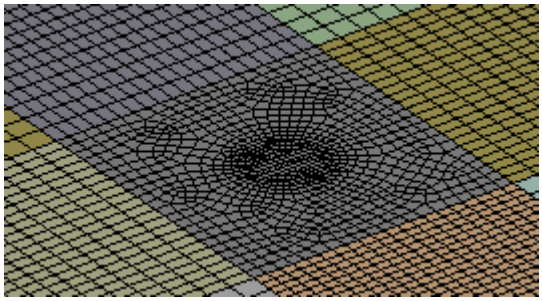

(a) (b)

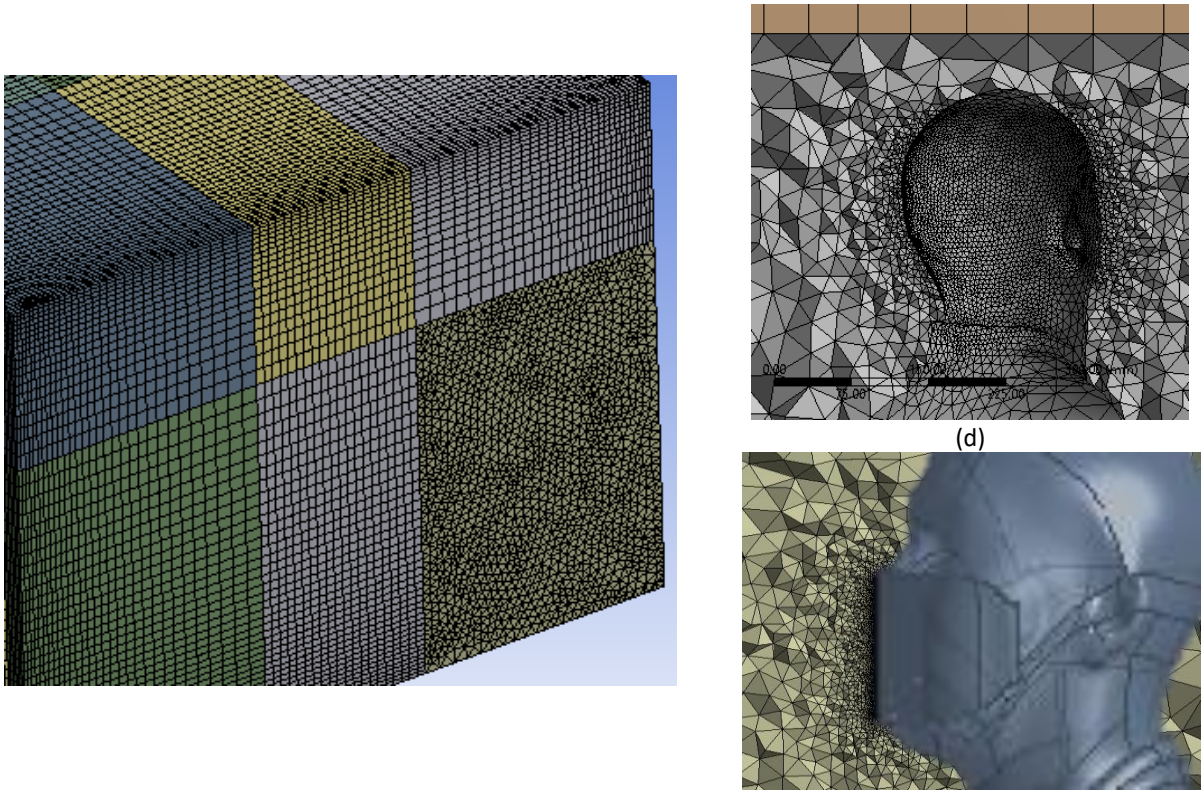

(c) (d) (e)

Figure 2: Details of selective meshing for the different segments of flow domain (a) unstructured hexahedral elements at the discharge ports (b) at the air inlet ports (c) tetrahedral elements at segment with mannequin and (d) mesh size refinement around mannequin's face without facemask (e) mesh size refinement around facemask

In order to mesh the flow domain in the two rooms, selective meshing was carried out (using Ansys Meshing® v19.2) for each of the 36 segments created by slicing each room into 18 segments. An unstructured mesh was created in the segment containing the mannequin using tetrahedral mesh elements. Tetrahedral mesh elements are best suited for domains containing complex or irregularly shaped geometries such as the mannequin. All other segments were meshed either with hexahedral or hybrid hexahedral-prism elements. Such hybrid meshing techniques have proven computationally efficient in many fluid flow applications [32]–[36]. Due to the presence of the inlet and outlet air ducts, segments containing these were meshed with hybrid elements while the others were meshed with purely structured hexahedral mesh elements. These are shown in Figure 2 (a–c). Refinements of the mesh were created around the face of the mannequin where the droplets are injected into the domain with elements that are 10% of the size of those in the bulk domain. For the case with the facemask, where there are holes of 0.6 mm in size, the elements there were 2% of those in the bulk domain to capture the flow of droplets that may escape the facemask into the room (Figure 2 (d–e)). Body sizing was applied in all segments to produce mesh elements in the bulk domain far from the mannequin, inlet and outlet ports that are 20, 30, and 50 mm in size.

2.2 Setup

2.2.1 Airflow simulation

The simulation of airflow in the rooms were carried out based on the steady formulation of the Reynolds Average Navier-Stokes (RANS) set of partial differential equations for mass and momentum conservation. The simulations were carried out using Ansys Fluent (v19.2). The two-equation k-ε RNG turbulence model was selected which was demonstrated by several authors [37]–[39] to be robust and stable for single-phase airflows in indoor environments. Pressure-velocity coupling was achieved

using the Coupled scheme. The second order upwind scheme was used for the discretisation of pressure, momentum, turbulent kinetic energy, and dissipation rate. Convergence was considered to have been reached when the residuals were less than 10^{-4} for the flow variables (continuity, x-, y-, and z- velocities, k, and ε) and 1000 iterations were required to reach steady state. Simulations were performed on a Windows desktop computer with a 3.0 GHz Intel Quad Core Processor with 32 GB RAM. The operating system was Windows 10 Professional 64 bit and calculations required approximately 4 hours for the mesh selected. For the boundary conditions, the mass flow rate of air going into the rooms through each of the inlet ports at the top of the rooms was set at 0.1 kg/s. This value corresponds to 4 air changes per hour (ACH) in domestic settings. For the discharge ports, pressure outlet was set as the boundary condition. All other boundaries in the domain were set to wall and no-slip boundary condition was imposed including the mannequin. Furthermore, for DPM purposes, the walls were set to "trap" to prevent elastic collisions of the liquid droplets upon contact with the surfaces. The simulation settings are summarised in Table 1. Finally, the temperature of the room and inlet/outlet air flows were kept constant at 25˚ C (298.15 K) for all the simulations carried out in the study.

Table 1: CFD solution setup settings

Setting	Value
Steady/transient	Steady (RANS)
Turbulence model	K-epsilon
Dispersed phase model	DPM
Inlet boundary condition	Mass flow inlet (0.1 kg/s)
Spatial discretisation	2nd order upwind (continuity, momentum, k and ε equations)
Gradient method	Green-Gauss node based
Pressure-velocity coupling	Coupled scheme
Convergence residuals	10^{-5}

2.2.2 Mesh independency study and validation

A mesh independency study was carried out using mesh with different element sizes. It showed that the mesh with 50-mm sized elements (19 million elements in total) produced only a 5% difference in the source room's inlet/outlet static pressure drop when compared with the finer 20-mm sized elements (25 million elements in total). Therefore, the mesh with 50 mm elements was selected and used to carry out the simulations presented in this paper. For computational efficiency, the unstructured tetrahedral elements were converted to polyhedral which reduced the number of elements to 5.1 million.

In order to validate the airflow simulations, we have matched the experimental data of Kalliomaki et al. [22] who performed measurements in the same building geometry as used in this paper. In their experiments, an imbalance in the inlet and outlet air flow rates in each room was created. The inlet and outlet volumetric flow rates in the inner room were 176 L/s and 194 L/s respectively, giving an excess discharge of 18 L/s corresponding to air mass flow rates of 0.2156 and 0.2377 kg/s.

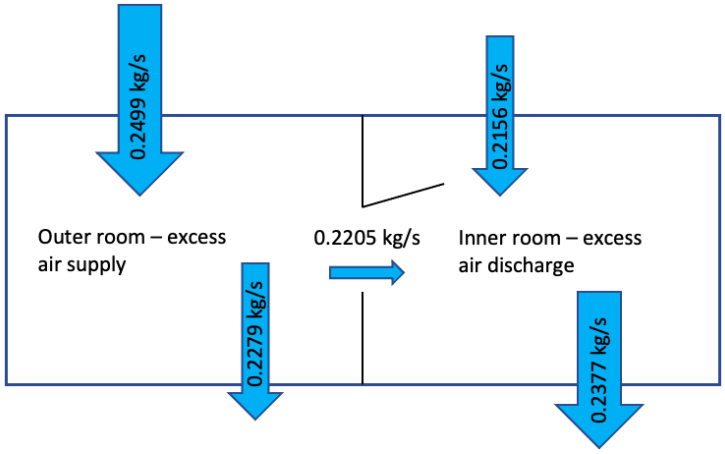

Figure 3: Illustration of flow rates used for validation from Ref. [22] showing the supply and discharge air flow rate differentials along with the induced net flow through the door for negative pressure generation in the inner room.

Conversely, the inlet and outlet volumetric flow rates in the outer room were 204 L/s and 186 L/s respectively, giving an excess intake of 18 L/s corresponding to air mass flow rates of 0.2499 kg/s and 0.2279 kg/s (Figure 3). With these flow rates, a negative pressure difference of 20 Pa existed once the door was closed. For the validation exercise, we carried out two simulations: one with the connecting door open in order compare the mass air flow rate through the door, and the other with the doors closed for comparing the pressure difference between the rooms.

Table 2: Comparison of current simulation results with experimental data of Kalliomaki et al. [22]

Quantity	Current simulations	Experimental data of Kalliomaki et al. [22]	Percentage difference
Air flow rate through doorway (kg/s)	0.2181	0.2205	-1.1%
Static pressure difference (Pa)	20.7	20	+3.5%

Table 2 shows a comparison between the results of the simulations carried out and the experimental data of Kalliomaki et al. [22]. It indicates that there is a 1.1% difference between the simulated and experimental volumetric air flow rate through the door. Furthermore, there is a 3.5% disparity between the simulated and experimental static pressure difference of the inlet and discharge ports of the rooms. Based on these findings, the simulation results were validated which in turn provided confidence in proceeding with the mesh and setup for further analysis.

2.2.3 Discrete phase modelling

The discrete phase model (DPM) solves the transport equations for a dilute discrete second phase flowing within a continuous phase. It calculates the velocities and trajectories of these entities, which could be liquid droplets in a gas, gas bubbles in a liquid, or solid particles in a gas, in a Lagrangian reference frame [40], [41]. The DPM method integrates the force balance on the particle. This force balance relates the particle inertia with the forces that act on the particles and is given as:

$$\frac{du_p}{dt} = F_D(u_g - u_p) + \frac{g(\rho_p - \rho_g)}{\rho_p} + \frac{1}{2}\frac{\rho_g}{\rho_p}\frac{d}{dt}(u_g - u_p) \quad (1)$$

where u_p and ρ_p are the particle velocity and density respectively; u_g and ρ_g are the continuous phase (gas) velocity and density respectively; g is acceleration due to gravity; and F_D is the drag force experienced by the particle and for a spherical particle is given by:

$$F_D = \frac{18\mu}{\rho_p d_p^2}\frac{C_D Re}{24} \tag{2}$$

where μ is the viscosity of the continuous phase, d_p is the particle diameter, and C_D is the drag coefficient which is related to Re (the relative Reynolds number), and is given by:

$$C_D = \frac{K_1}{Re} + \frac{K_2}{Re} + K_3 \tag{3}$$

with the coefficients K_1, K_2, and K_3 regression constants obtained when the equation is fitted to experimental data for particles that are spherically shaped or otherwise. Data for spherical particles is reported by Morsi and Alexander [40]. The relative Reynolds number (Re) is defined as:

$$Re = \frac{\rho d_p \left| u_p - u_g \right|}{\mu} \tag{4}$$

The third term in Equation (1) is the "virtual mass" force which is the force required to accelerate the fluid surrounding the particle and only is important when the continuous fluid is denser than the discrete phase. In the current case, that is not the case. Other forces that may be included in Equation (1) are forces due to rotating reference frames, and temperature change (i.e., the thermophoretic force) but these are for cases such as those found in turbomachinery and heated systems, respectively. Substituting Equations (2) and (3) into (1), the governing equation describing the motion of the discrete droplet phase is given as:

$$\frac{du_p}{dt} = \frac{18\mu}{\rho_p d_p^2}\frac{Re}{24}\left(u_g - u_p\right)\left(\frac{K_1}{Re} + \frac{K_2}{Re} + K_3\right) + \frac{g\left(\rho_p - \rho_g\right)}{\rho_p} \tag{5}$$

Integrating Equation (5) once and twice gives the particle velocity and trajectory, respectively. The discrete phase modelling approach has shown remarkable robustness in previous works and several authors [42], [43] have adopted it for modelling the discrete phase in various flow systems.

2.2.4 Droplet size distribution and initial velocities

The initial velocities of expelled droplets by sneezes and coughs to be used in initialising the DPM simulations were determined from the literature. Tang et al. [44] obtained cough velocity maps using Schlieren photography with images captured at 3000 frames per second. A maximum velocity of 8 m/s was obtained by averaging instantaneous realisations over a period of 0.5 s. Kwon et al. [45] used particle image velocimetry (PIV) to measure velocity at which coughs and sneezes were expelled from male and female subjects. Atomised oil droplets were used as droplets and tracing particles for the velocity determination in the PIV algorithm. They reported initial cough velocities of approximately 11 and 15 m/s for females and males, respectively. Furthermore, Chao et al. [46] also carried out PIV experiments to determine coughing velocities. Unlike the work of Kwon et al., no oil mist was used but an interferometric Mie imaging (IMI) technique was used to determine ejected bio-mist initial velocities. They reported an average initial cough velocity of 11.7 m/s. In terms of sneezing, Scharfman et al. [47] studied human sneezing by analysing high-speed video recordings and reported droplet velocities of 14 m/s with ligaments reaching velocities of up to 35 m/s. Therefore, coughing and sneezing produce liquid droplets of different initial ejection velocities that can range from 5 to 15 m/s for coughs and up to 35 m/s for sneezes. In order to study the transport mechanisms of the different droplets from cough and sneezes, we used 5, 10 and 15 m/s for initialising cough simulations and 15, 20, and 25 m/s for sneezes in the current simulations.

Typical droplet size distributions characterising the size ranges for coughs and sneezes have been reported to be remarkably variable. These are experimental studies that were reported on the characterisation of cough and sneeze droplets using human subjects. The studies show that exhaled droplet distributions can either be unimodal [48]–[50] or multi-modal [5], [44], [51], [52]. In an experimental study, Han et al. [52] carried out droplet size experiments of sneezed droplets exhaled by 20 healthy subjects where a total of 44 sneezes were measured using a laser particle size analyser. Their results show that sneezed droplets were multi-modally distributed between 20 and 1000 µm for all the subjects. For the experiments carried out by Ward-Smith [51] using a laser diffraction particle analyser, they also reported a multimodal distribution with a similar size as that of Han et al. [52]. For coughs, Ward-Smith [51] reported the droplet size distribution ranging from 70 to 1000 µm with a median droplet size of 450 µm. Their measurements were carried out using laser diffraction. Obtaining the average droplet sizes and overall size range is important as they will be used to approximate the parameters of the Rosin–Rammler distribution which is given by:

$$Y_d = e^{-(d/\bar{d})^n} \tag{6}$$

where Y_d is the fraction of droplets of diameter *d*, n is the shape or spread parameter, and $\bar{d}$ is chosen as the particle diameter at which $Y_d = e^{-1} = 0.369$. The Rosin–Rammler distribution was used to specify the droplet injection size distribution. The data of Duguid [53], shown in Figure 4 (a) which was also used by other authors [49] for sneezes and coughs was adopted. The number of particle size ranges used in the simulations were 200 meaning the particle sizes are uniformly binned at intervals of 10 µm and a spread parameter was found to best fit both sneeze and cough droplet size data sets from the data of Duguid [53].

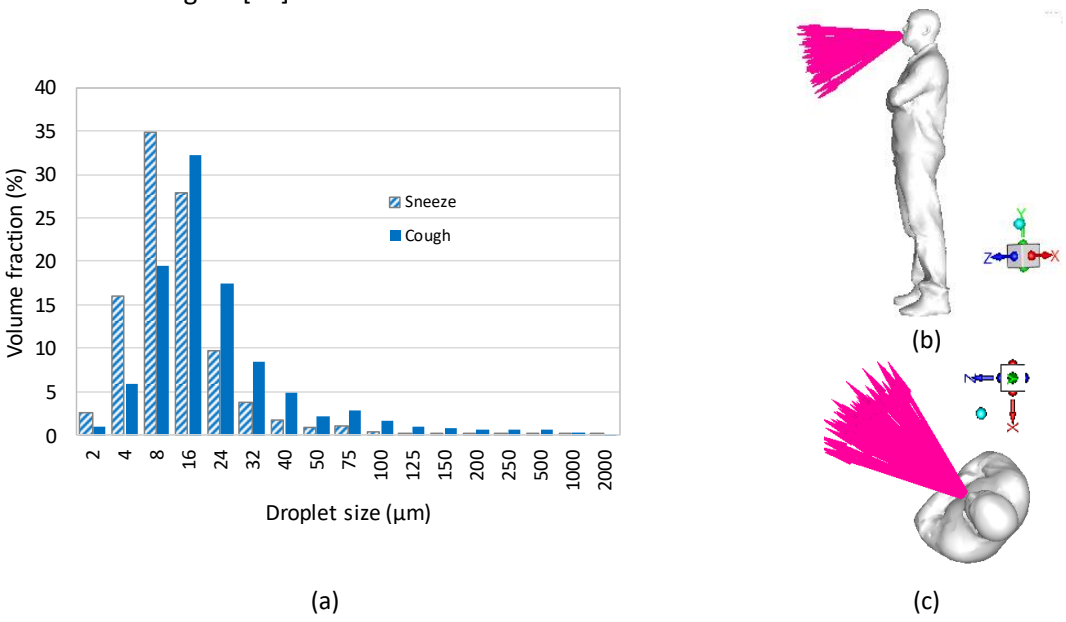

Figure 4: (a) Cough and sneeze droplet size distributions used for specifying the Rosin-Rammler distribution of the cone injection in our simulations (from Duguid [53]**) (b) side view of cone injection's geometry of ejected droplets with respect to mannequin (c) top view showing mannequin and injection**

Figure 4 (b and c) shows the location of the cone injection of droplets 1 mm from the mannequin surface to prevent any of the particles being outside the flow domain. Bourouiba et al. [49] noted that droplets expelled at the mouth during sneezing and coughing actions can follow widely varied expiratory directions, which may be because of complex oral cavity differences in humans such as the effects of teeth and head movements. We therefore set the spread angle of the cone at ± 20° from its axis, as per experimental measurements of coughs conducted by Wei and Li [54] where they observed

a characteristic angle of 20.8°. The cone axis is itself is angled at -20° from the horizontal and an initial cone radius of 15 mm was set based on a similar size used by Wei and Li [54]. Furthermore, the droplet injection was made as a full 360-degree circular cone originating from the mouth area. A range of cough and sneeze droplet size as well as initial exhalation velocities were decided as per the earlier discussion and are as shown in Table 3. As can be seen in the table, the range of cough and sneeze droplet sizes are from 1 to 2000 µm, with a mean size of 32.6 µm for cough and 17.5 µm for sneezing. The velocity ranges were defined as 5–15 m/s for coughing and 15–25 m/s for sneezing (based on the reported works of refs [44], [45], [47]).

Table 3: Range of velocities and droplet sizes used for simulations.

Quantity	Value	References
Droplet size distribution		
Cough	Range: 1 – 2000 µm, Mean: 32.6 µm	[53]
Sneeze	Range: 1 – 2000 µm, Mean: 17.5 µm	
Droplet ejection velocity		
Cough	5, 10, 15 m/s	[44], [45], [47]
Sneeze	15, 20, 25 m/s	

3 Results and discussion

The following section qualitatively and quantitatively describes the droplet transport characteristics from the source to the second room. Analysis is made on the effect of the facemask during the various coughing and sneezing scenarios simulated.

3.1 Airflow pattern in room

The air ventilation simulation in the room was allowed to run in steady mode for 1,000 iterations for convergence. Contours of velocity magnitude are shown in Figure 5 (a) and the streamlines of airflow are given in Figure 5 (b). These are at the central plane of symmetry that passes through the two air inlets, at the mannequin and one at 0.05 m parallel from the outlet ports. As expected, the contours show the inlet air as axisymmetric air jets with the highest velocities of around 2.3 m/s at the inlet ports. The air decelerates progressively as it descends towards the floor and spreads around each room at very low velocities (less than $1/10^{th}$ of the inlet) and only accelerates towards the discharge ports. In essence, except for the occupants that are in direct path of the inlet ports, the intensity of the blowing air at this flow rate (4 ACH) is not felt, for example at the location where the mannequin is situated. However, it is expected that exhaled micro-droplets by an individual at that location can be transported around the room, possibly to the adjoining room and discharging at the vent ports with some deposition within the rooms. The extent to which this happens is studied in more depth in the following section.

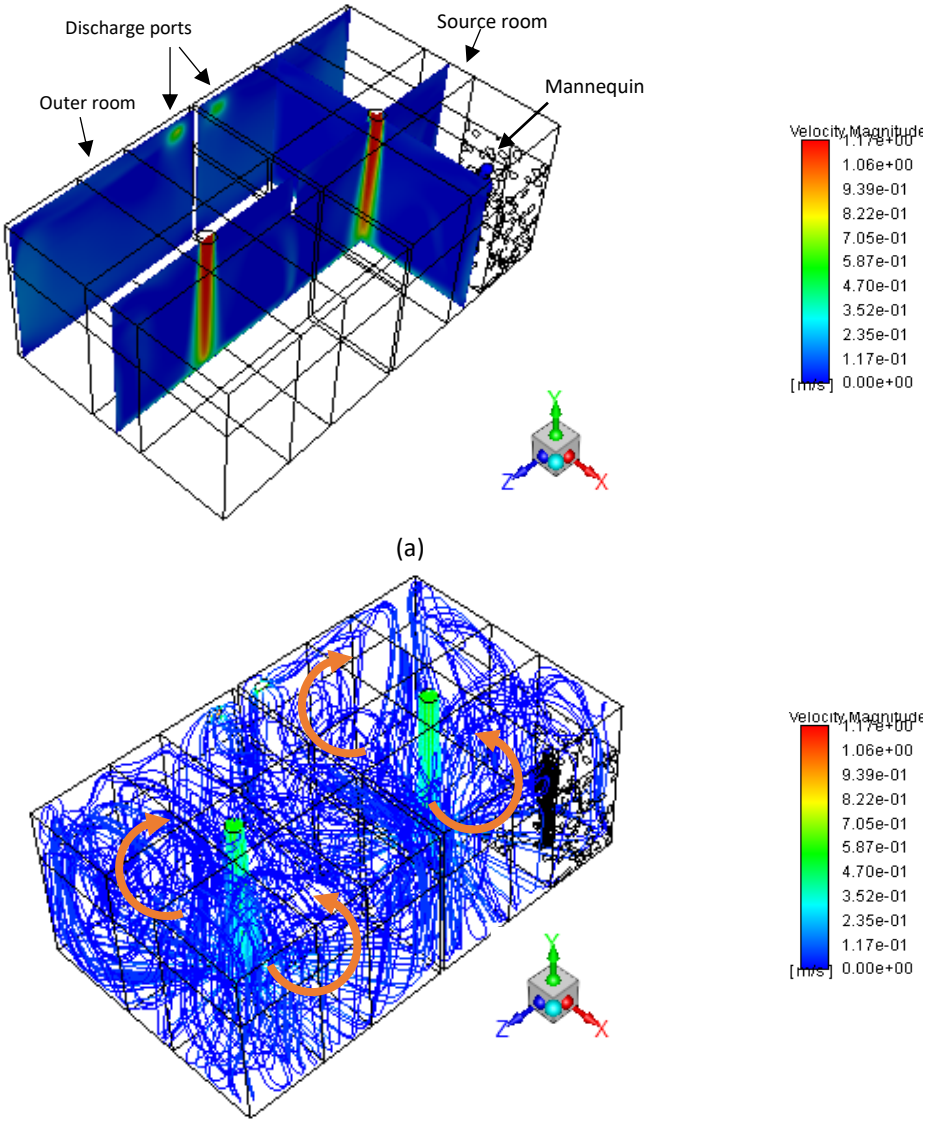

Figure 5: (a) Air velocity contours on central plane, at the mannequin and near the exhaust ports (b) Streamlines of air flow in rooms (coloured by velocity magnitude) showing inlet ventilation from overhead ports and exit at vent ports. The orange arrows show the general circulation pattern of the air flow.

3.2 Droplet migration

Ejected droplets due to coughing and sneezing produce droplets of different sizes and velocities. These can have significant impact on the transportation or migration characteristics at the vicinity of the source subject and also within the far field of the confined spaces they are located. Figure 6 shows the initial ejection of droplets during coughing and sneezing actions at an initial velocity 15 m/s. The droplets tracks are represented by proportionately sized spheres and coloured by droplet size. It is seen that coughing action while producing larger droplets (up to 270 μm) than the sneezing action (up to 51 μm), also produces droplets that disperse farther before their initial momentum is overcome by the draft in the room caused by the ventilation. In both cases, the smaller droplets can also be seen to be transported nearer the subject than the larger ones due to the momentum difference between droplets of different sizes because of their masses. We also observed that lower droplet flow velocity e.g. cough at 15 m/s reduces particle dispersion and was equally reported by Leonard et al. [55].

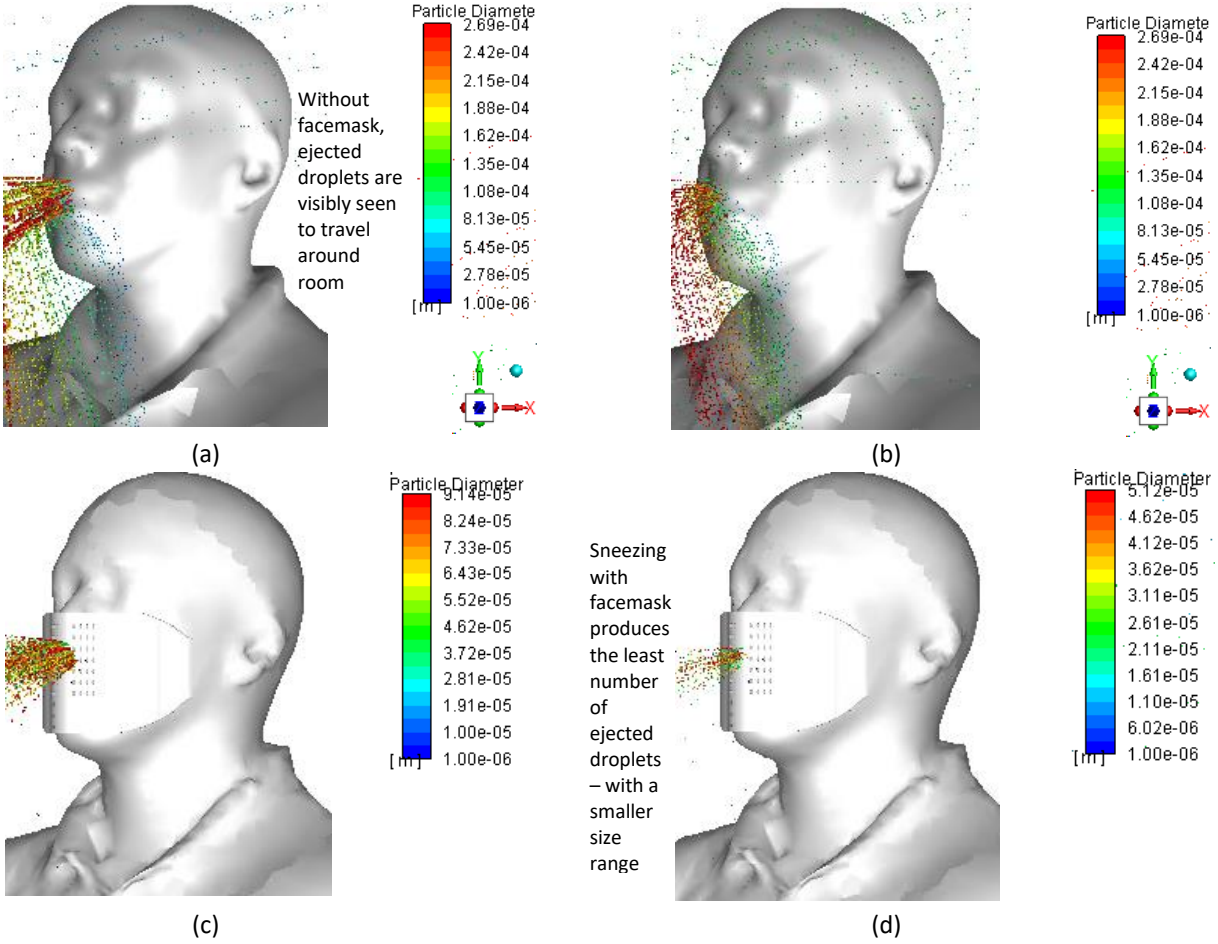

Figure 6: visualisation of ejected droplets during (a) coughing (b) sneezing without facemask and (c) coughing (d) sneezing with mask all at an initial velocity of 15 m/s.

Droplets that deposit in the immediate surrounding of the source subject are clearly the larger ones as shown in the images in Figure 7 for all no facemask simulated cases of coughing and sneezing. For the 5–15 m/s coughing cases, there does not appear to be a significant difference in the spatial distribution of the large droplets as they disperse from the mouth to the ground as seen in figures a–c. The same can be said for the sneezing cases. However, the difference is clear when coughing is compared with sneezing. Even though for sneezing the droplets are more finely distributed, the trajectories of the larger droplets in both situations are largely the same. The track for the large, sneezed droplets is less clearly defined than that of coughing even though the total number of droplets ejected for sneezing is twice those of coughing. Further analysis of the deposited droplets on the ground that is in the vicinity of the mannequin is given in the succeeding discussion where particle data was extracted within a 2 m radius around the mannequin. This area represents the area where social distancing is advised to prevent direct deposition of ejected bio-droplets on persons around the source individual.

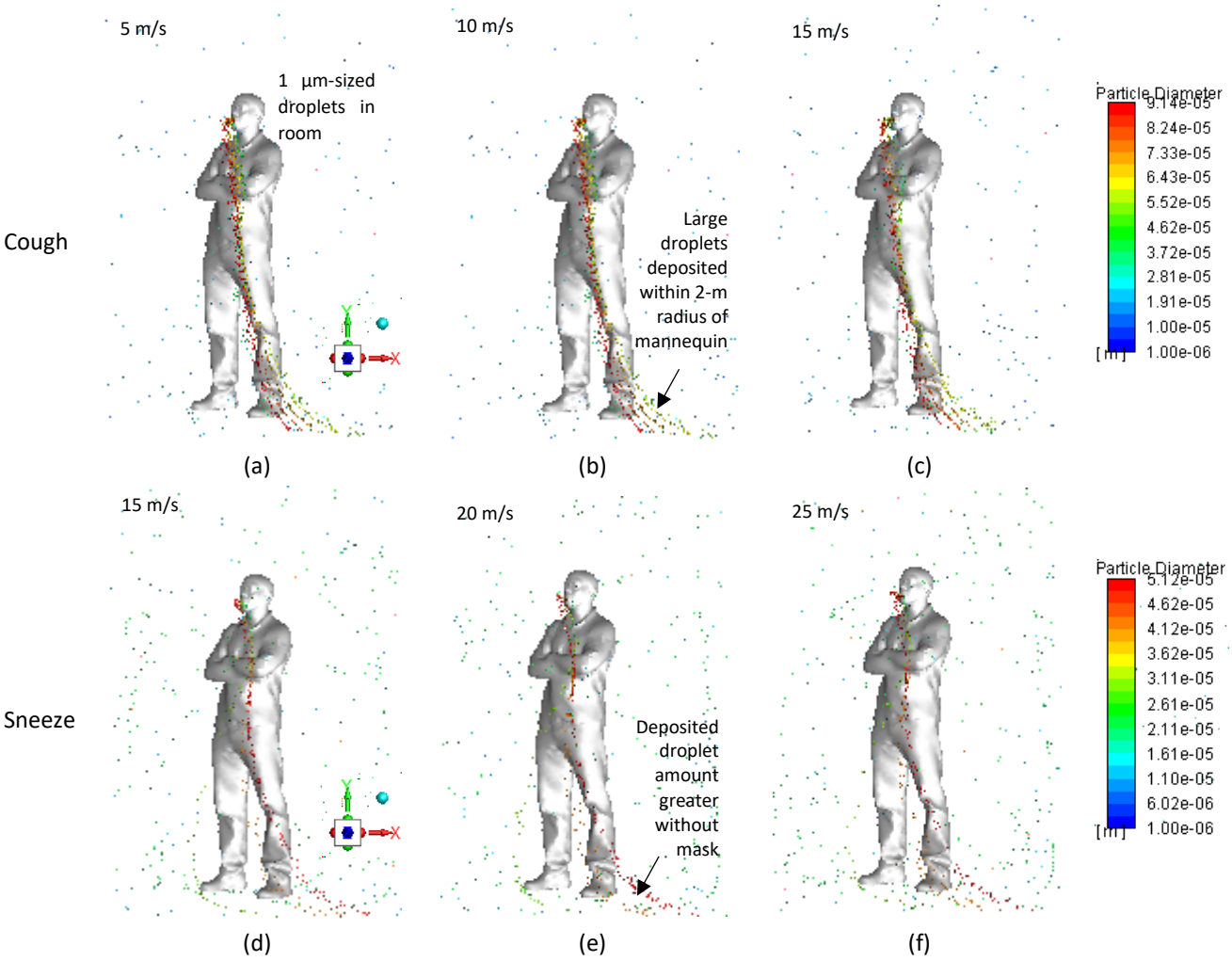

Figure 7: Visualisation showing ejected droplets for coughing and sneezing without facemask.

In contrast, the facemask cases show remarkably reduced airborne droplets (Figure 8) especially for the coughing cases which contain half the number of droplets as sneezing. Airborne droplets around mannequin, visible in the no facemask scenarios, are almost non-existent in the cases with a facemask. This shows the efficacy of using facemasks, albeit porous homemade ones, in reducing the emission of bio-aerosols and potential transmission from infected persons.

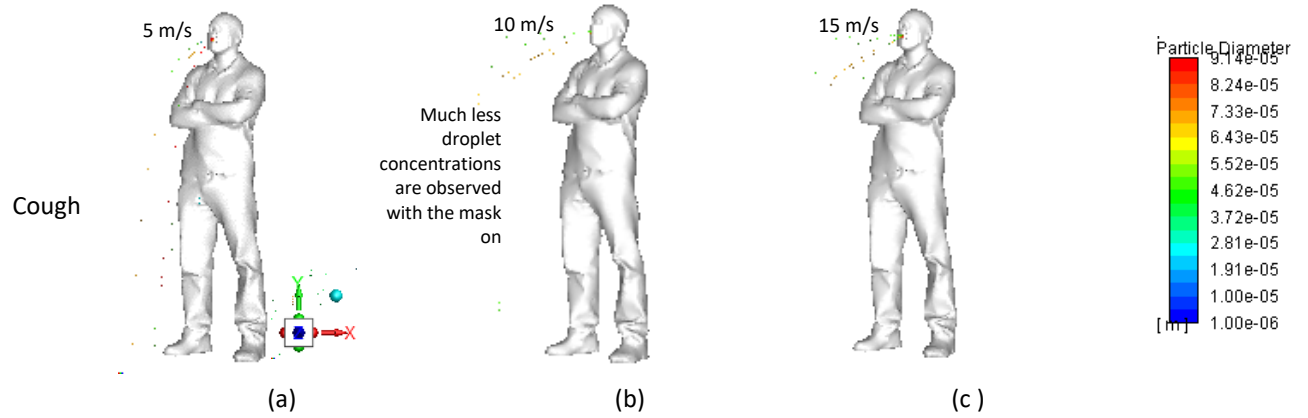

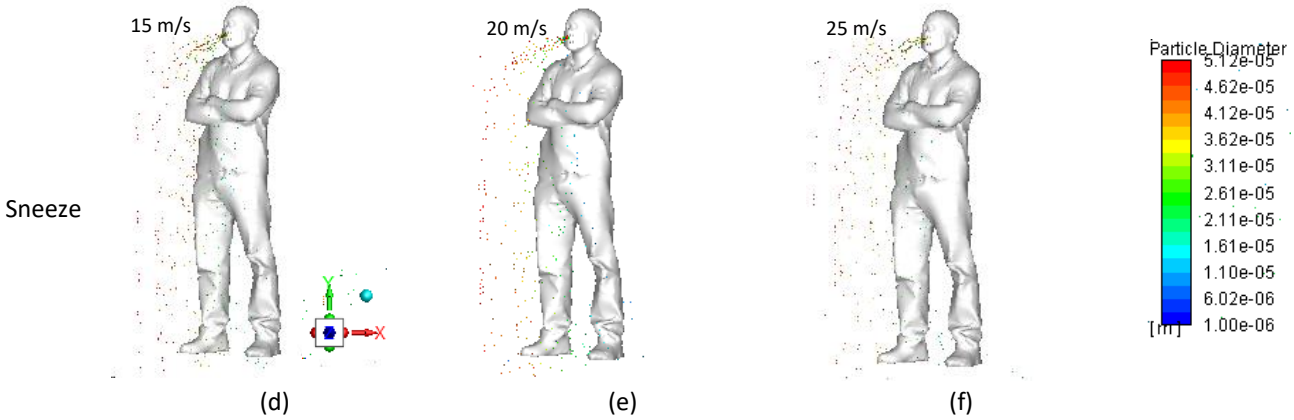

Figure 8: Visualisation showing ejected droplets for coughing and sneezing with facemask.

The plots in Figure 9 depict the fractions (on the vertical axis) of the various droplet sizes (on the right horizontal axis) that were deposited on the floor around the mannequin or that cross the door to the outer room for the various cough and sneezing conditions simulated. The fractions were calculated based on the total number of droplets ejected. Figure 9 (a) shows the distributions of droplets that were deposited in the 2 m radius around the mannequin. It can be seen that the deposited droplet distributions for the three sneezing cases are similar in terms of their fractions and size range (10–300 µm). The same can be said of the similarity between the coughing cases, but their droplets have a wider size range (10–1110 µm). Between coughing and sneezing, the difference in the shapes and ranges of droplets of both distributions is clear, the sneezed droplets single-peaked but the coughing droplets are with a wider range of droplet sizes that are deposited within the 2 m radius around the mannequin. Crucial however, is the absence of the smallest droplets (< 10 µm) being deposited in the immediate vicinity of ejection. These are transported further afield around the room and beyond, meaning that the dispersion process is more controlled by droplet size than by ejection velocity. Inspection of Figure 9 (b) provides evidence that this is indeed the case. It shows the distribution of droplets that crossed the door and transported to the outer room. The droplet sizes in both sneezing and coughing are remarkably similar – both are bimodal and peak at 1 and 10 µm for both cases with the former being dominant suggesting that droplet size rather than ejection type (cough or sneezing) is more controlling in droplet transfer. Furthermore, the size of transported micro-droplets transported to the far field fall within the range of droplet nuclei (less than 5 µm in size) and that of respiratory droplets. Droplets within these size ranges have been identified [1] as the vehicles for the transfer of infectious respiratory diseases such as those transmitted by coronaviruses.

Figure 9 (c) shows the distribution of droplets that were deposited in the 2 m radius around the mannequin with the facemask on. Similarly, as with the no facemask case, the deposited droplet distributions for the three sneezing cases are similar in terms of their fractions and size range (10–90 µm). There is also a similarity between the coughing cases whose droplets, however, have a wider size range (10–120 µm) deposited. In general, there is a clear difference in the shapes and ranges of droplets of both distributions.

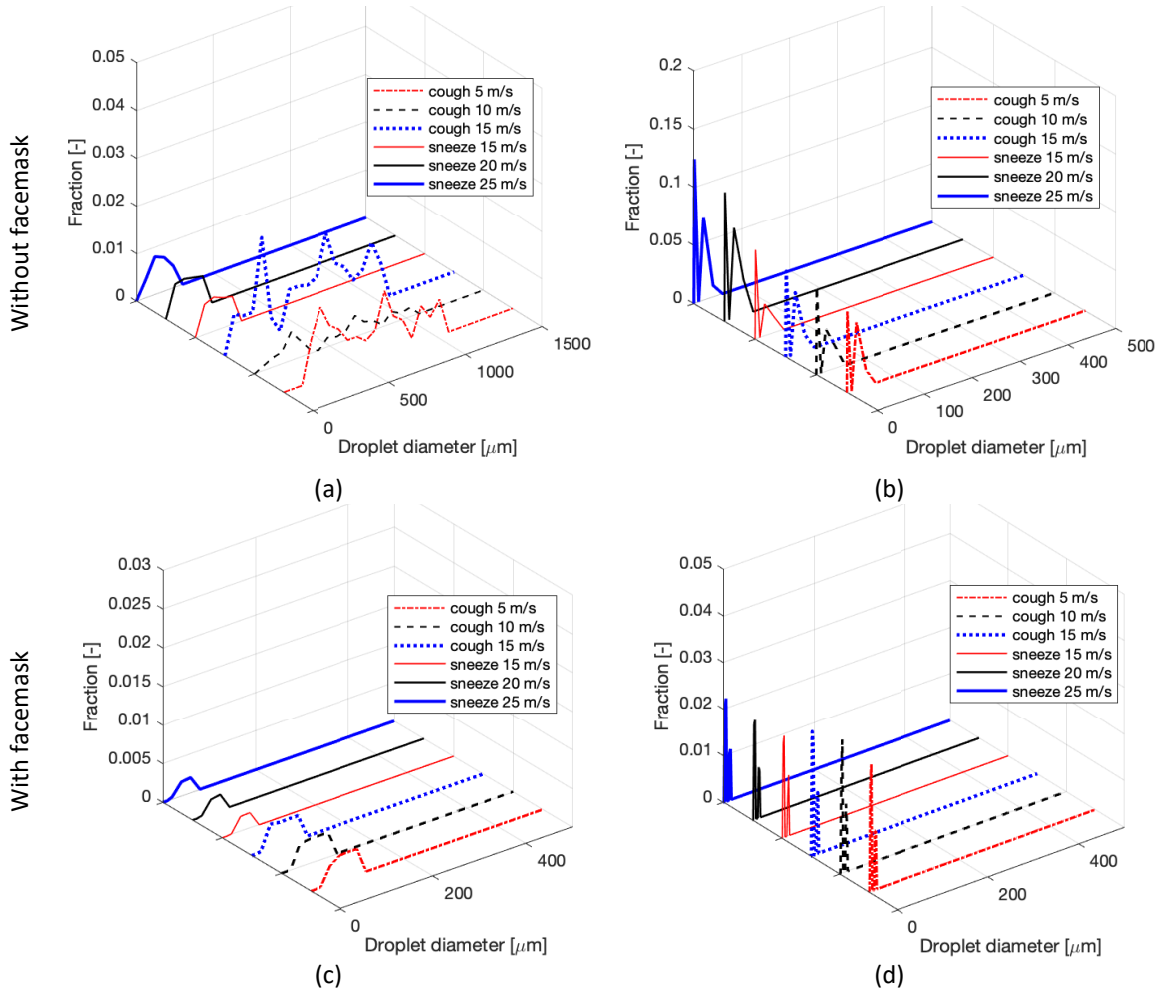

Figure 9: Distributions of droplet sizes (a) deposited on floor within 2 m radius of source (b) that migrate through door to ante room without facemask and (c) deposited on floor within 2 m radius of source (d) that migrate through door to ante room with facemask. Fractions were calculated based on the total number of droplets coughed or sneezed.

The deposited sneezed droplets are unimodal, but the coughed ones are distributed over a wider range of sizes in the 2 m radius around the mannequin. This is similar with the no facemask case only that the biggest difference is in the larger sizes of the droplets coughed which are with diameters that are larger. Again, similar to the no facemask case, there is the absence of the smallest droplets (< 10 µm) being deposited in the immediate vicinity of ejection. These are transported further afield around the room, through the door and into the other room before they leave the rooms through the discharge ports. Figure 9 (d) shows the distribution of droplets that pass through the door to the ante room for the cases with the facemask. Only droplets of 1 µm cross the door to the ante room with the facemask for both sneezing and coughing, further suggesting droplet size being the controlling parameter for droplet transport. The size is within the 1-5 µm bio-aerosol range that constitute droplet nuclei and have been acknowledged by WHO [1] to be virus-laden and transmit respiratory diseases.

We next quantify the number of droplets transported or immediately deposited. Figure 10 (a) shows the fraction of ejected droplets that have migrated from the source to the adjoining ante room as well as the fraction of droplets trapped on the floor surface that is within the 2 m radius of the mannequin. Plotted on the horizontal axis is the dimensionless initial velocity $u_i{}'$ where the sneeze or cough initial velocity u_i is non-dimensionalised by the maximum initial sneeze velocity $u_{i,snz,max}$ such that $u_i' = u_i/u_{i,snz,max}$. For coughing, 72.9, 76.9, and 78.8% respectively of droplets ejected fall directly to the floor within the 2 m radius area around the source. As previously shown, these are the larger

droplets of 20 µm size and above. Conversely, 10.5, 12.8 and 13.9% of the coughed droplets are carried with the airflow and migrate through the door to the ante room. This means that only 16.6, 10.3 and 7.3% of droplets are airborne in the source room before getting discharged through the vent. For sneezing, 61.4, 61.6 and 64% of droplets ejected for the three initial velocities fall to the ground around the mannequin and consist of droplets within the range of 10–90 µm. Additionally, 21.7, 21.8 and 17.5% of sneezed droplets are transported through the door to the ante room, leaving 16.9, 16.6 and 18.8% of droplets airborne in the source room before being discharged through the vent port.

A different picture of droplet transport emerges for facemask sneeze and cough cases. As shown in Figure 10 (b), between 90 and 91% of all droplets are trapped in the facemask. In fact, 96–97% of the ejected droplets are either trapped in the facemask or deposited on the 2 m radius floor space around the mannequin. This further reinforces the importance of using face coverings (even porous cloth masks) in limiting the extent of infected micro-droplet transfer to other individuals.

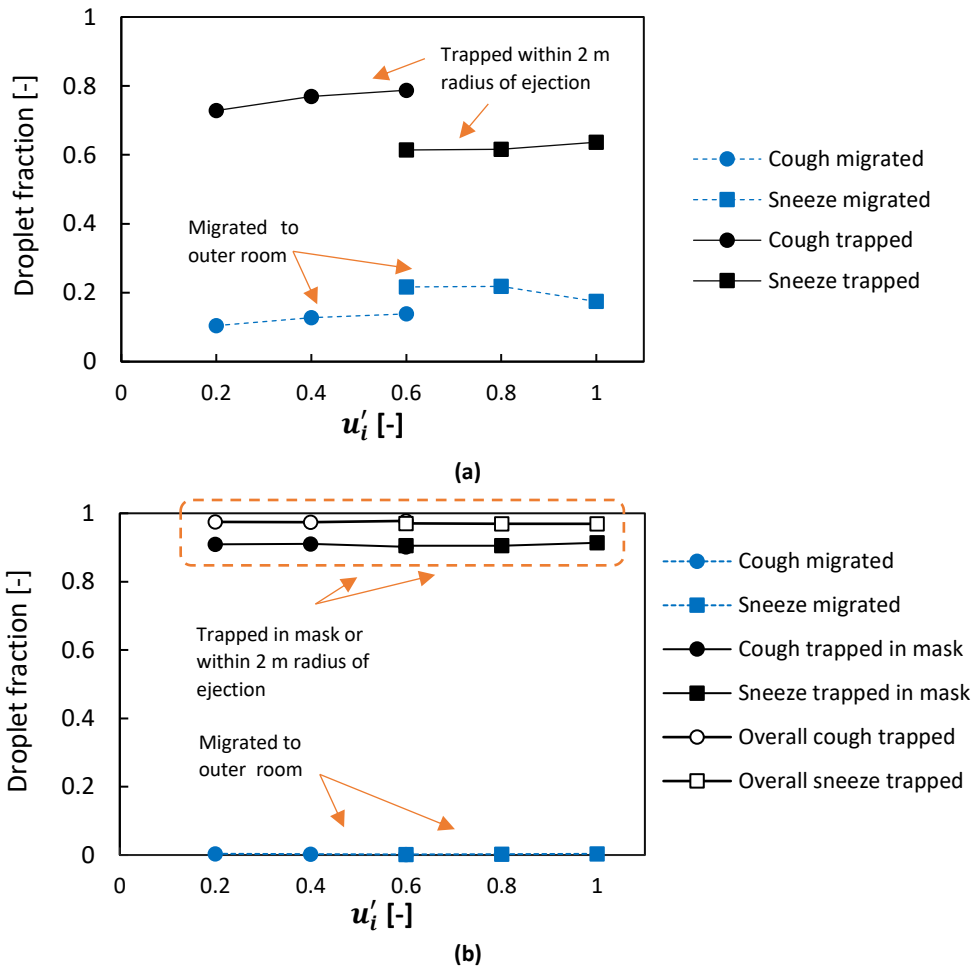

Figure 10: Droplets trapped within 2 m radius of source and those that migrate through door to ante room as quantified by trapped and migration fractions respectively (a) without facemask (b) with facemask

In order to understand the extent of micro-droplet transfer from source to ante room, droplet tracks were produced for the entire flow domain that consists of both rooms. These are shown in Figure 11 for all the cases considered, with the droplet tracks coloured by droplet diameter. Only 100 particles are tracked to obtain maximum visual clarity in the figures. As can be seen, the droplet tracks consist entirely of the smallest droplets (of between 1 and 5 µm) which migrate to the ante room and whose tracks obscure those of the larger droplets deposited in the immediate vicinity of their source (at the bottom left of each figure). The coughing scenarios produced noticeably less dispersion through the

door to the ante room due to the droplet size and momentum considerations previously discussed. Figure 11 additionally shows that there is little difference in the droplet concentration in the inner room for most conditions of coughing and sneezing considered except at 5 and 10 m/s of coughing and 25 m/s of sneezing. Nevertheless, there is significant amount of micro-droplet transfer to the outer room. As such, both coughing and sneezing may cause similar levels of droplet transmission (without a facemask) and perhaps infection if the source is a carrier of a respiratory disease. Furthermore, droplet tracks reveal reduced concentration downstream of the door into the ante room. These are more visible towards the middle of the door and droplets escape nearer the door's edges than at the middle (indicated by the red oval in Figure 11). This behaviour can be attributed to the effect of ventilation pattern caused by the central location of the inlet ports which cause a circular air motion that radiate from the top of the rooms downwards and symmetrically towards the walls and upwards (see streamlines in Figure 5 (b)). It can be inferred that the upward draught that is created in either room by the downward ventilation affects the droplet dispersion pattern through the door from the source to the outer or ante room.

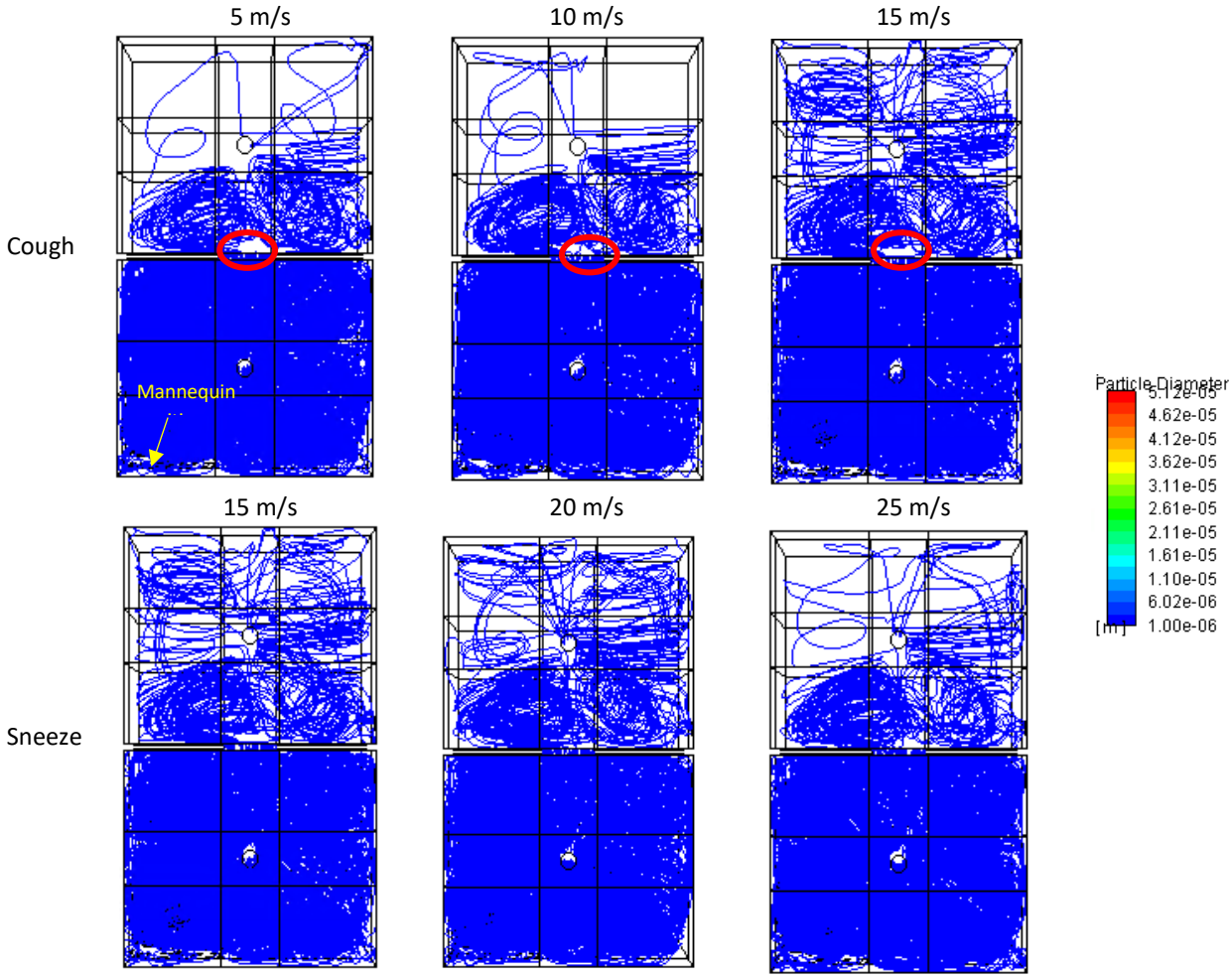

Figure 11: Top view of droplet streaks for the no facemask case studies, coloured by particle diameter (100 particles tracked)

In contrast to the no facemask scenarios, Figure 12 visually shows the significantly reduced number of droplets that are transported from the source when a facemask is worn. Again only 100 particles are tracked to obtain maximum visual clarity in the figures. For coughing, the density of droplet tracks appears to decrease with increasing ejection velocity. This may be due to droplets lacking sufficient momentum to deposit and hence more remain airborne. For the case of sneezing, increasing ejection

velocity does not produce a marked effect on track density in the source room which agrees with the plots in Figure 10 (b). Overall, the density of tracks is seen to be much reduced for the sneezing cases around the source room as well as those that travel through the door to the ante room, consistent with the plotted values.

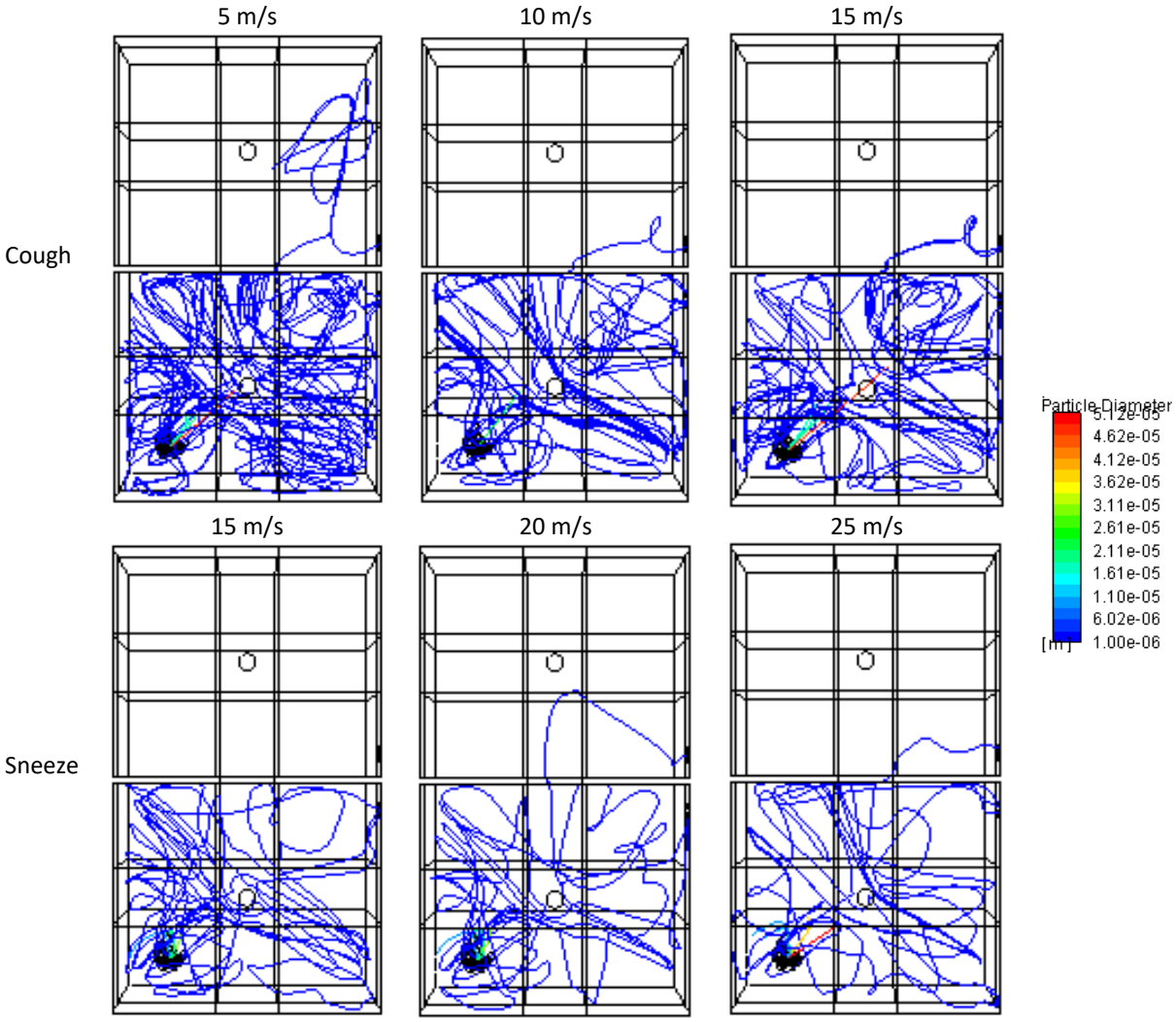

Figure 12: Top view of droplet streaks for the six case facemask studies, coloured by particle diameter (100 particles tracked)

To obtain more detail on the spatial distribution of droplets as they are transported to the ante room, Figure 13 shows droplets that were sampled at the door i.e., normal to the direction of flow between the rooms. For the no mask cases, there is a general stratification of droplets into two layers. A limited range of two droplet sizes are represented i.e., those that are 1–2 µm in size on the one hand and those that are 16–20 µm in size. These correspond to the two peaks seen in the droplet distributions presented in Figure 9 (b). it is seen that the stratification is generally not based on droplet size, as both the large and small droplets are interspersed with each other. However, the larger droplets are seen to be those closest to ground level and their concentration at those locations are higher than elsewhere across the door. Hence, the larger droplets are more likely to deposit than the smaller ones. This is consistent with the earlier assertion that droplet size (hence weight) has a dominant effect on their transportation or dispersion characteristics as the smaller droplets have more tendency to be transported than the larger ones. However, with the facemask cases, only the smallest (1 µm-sized) droplets get transported to the ante room. This again reinforces the importance of using face

coverings especially during respiratory disease epidemics or pandemics such as that of the SARS outbreak in 2009 and COVID-19 in 2019.

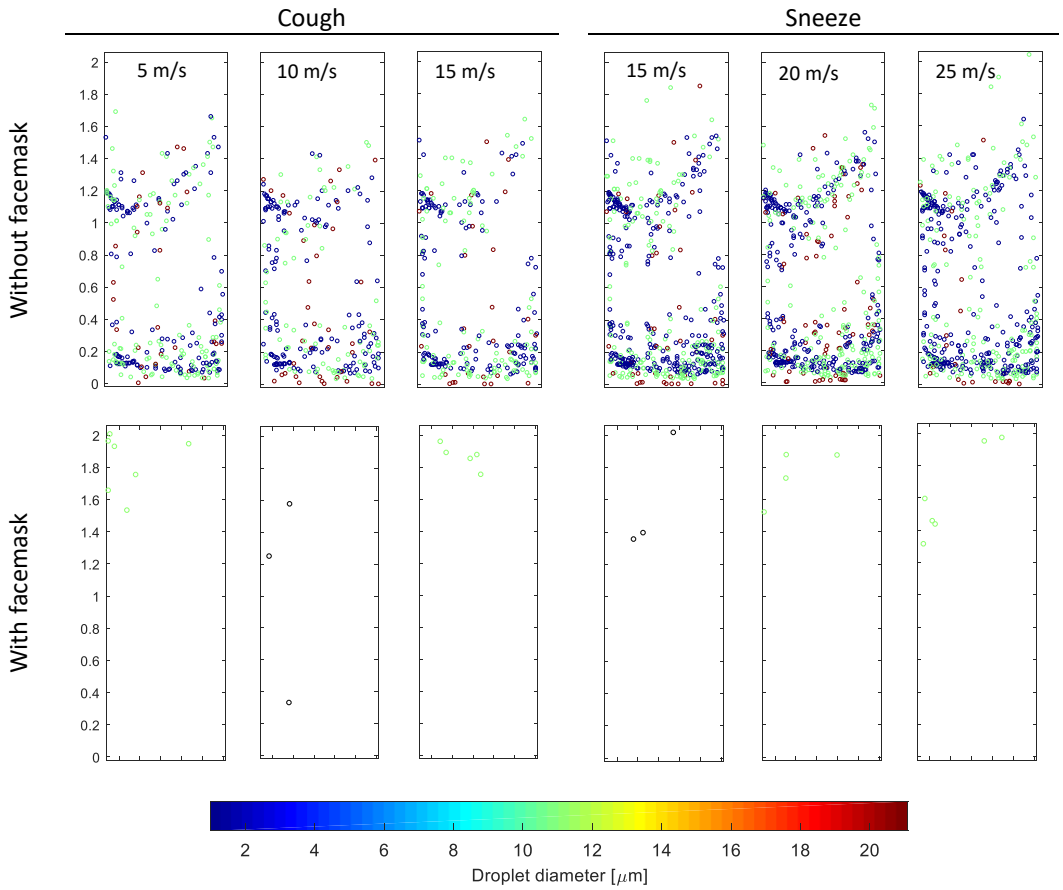

Figure 13: Spatial distribution of droplets migrating to ante room for each of the cough and sneeze initial droplet ejection velocities. Numbers on first figure indicate heights along door height in m.

3.3 Correlation of droplet concentration

Quantifying droplet propagation from a source through indoor spaces is important in understanding possible infection transmission. Accordingly, we extracted the concentration of droplets ejected by the source (mannequin) at eight different planes (namely plane-a, plane-b, …, plane f) normal to the direction of discharge. The planes are approximately 0.6, 1, 1.5, 2, 2.5, 3, 3.7, and 4.2 m from the mannequin as shown in Figure 14 (a). Along with the droplet concentration in kg/s, the velocities of the droplets were also extracted. As there is recirculation within the room due to the ventilation, droplets are likely to cross each plane more than once as was observed from the droplet IDs in the extracted data. In order to ensure that the information of unique droplets was used for the determination of total droplet flow rate at each plane, filtering was carried out so that only droplets travelling away from the mannequin were used (i.e., those entering the planes from the front). Additionally, filtering was also done based on droplet ID to ensure each droplet is considered only once.

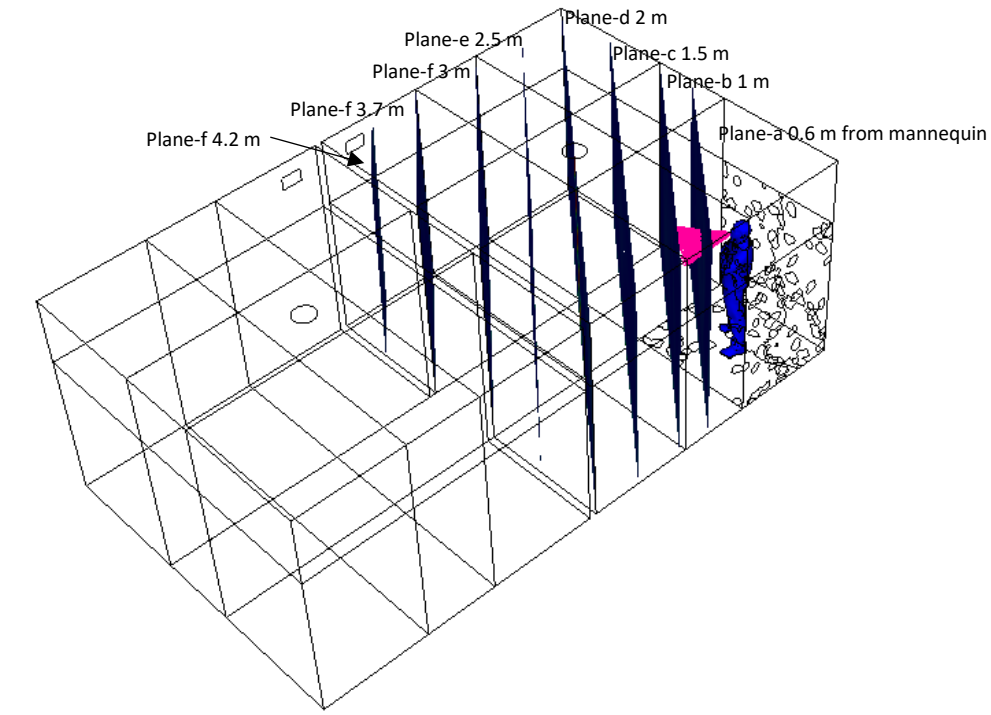

(a)

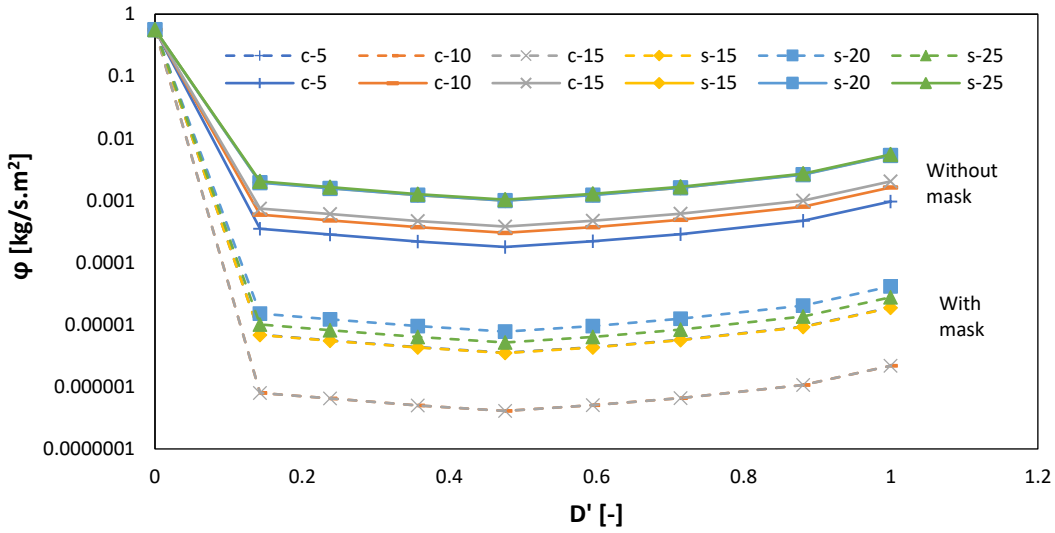

(b)

Figure 14: (a) Sampling planes for droplet concentration (b) Sampled data for droplet concentration expressed as a mass flux

Figure 14 (b) shows the droplet flux plotted as a function of the non-dimensional distance (D') from the mannequin or source. $D' = D_s/D_{max}$ is the non-dimensional distance from the source with D_s being the distance from source and D_{max} being the maximum sampling distance which is 4.2 m from the mannequin. The droplet flux is the droplet mass flow rate per unit area calculated by dividing the droplet mass flow rate $\dot{m}_d$ sampled on that plane by the area of the plane as follows:

$$\varphi = \frac{\dot{m}_d}{A_{plane}} \tag{7}$$

As can be seen, the droplet flow rate decreases rapidly from the ejected 0.56 kg/m^{2}s at the source to at least 10^{-3} and 10^{-5} kg/m^{2}s respectively for the cases with and without facemask, respectively. This Therefore, as expected, the facemask greatly reduces droplet flux, and the cough cases produce the

lowest amount with or without the facemask due to the presence of larger droplets which are mostly deposited either in the mask or in the vicinity of the mannequin. For all cases, a minimum droplet flux can be seen to occur at 2 m from the source indicating the droplet damping effect of the down-coming air jet from the source ventilation. As the droplets travel beyond the ventilation point at the centre of the room, there is a gradual increase in droplet flux. This is because of the droplets having an increasing velocity towards the outlet occasioned by the resultant droplet and air velocities being in the same direction as well as the suction provided by the pressure outlet at the exhaust port. In order to develop a one-dimensional model for the droplet concentration as a function of distance from the source, we note that the trend of the data in Figure 14 (b) can be represented with two exponential curves: an exponential decay from the source to the middle of the room and with an exponential growth curve from the middle of the room towards the exhaust port with a small growth constant, and both having the same asymptote. To do that, the droplet mass flux is non-dimensionalised as follows:

$$\varphi'(D') = \frac{\varphi(D')}{\rho_d \bar{u}_d(D')} \tag{8}$$

where ρ_d is the density of droplets and $\bar{u}_d$ is the mean droplet velocity at the appropriate distance from the source. Relationships for $\bar{u}_d$ were obtained by fitting the mean droplet velocities extracted at planes a–f to 8th and 7th order polynomials. The relationships, given in Equations (9) and (10), give the variation of the mean droplet velocities with distance from source. Without the mask it is given by an 8th order polynomial:

$$\bar{u}_d(D') = 3253(D')^8 - 14160(D')^7 + 25906(D')^6 - 25888(D')^5 + 15349(D')^4 - 5477(D')^3 + 1132(D')^2 - 121D' + u_{d,o} \tag{9}$$

and with the mask, by a 7th order polynomial:

$$\bar{u}_d(D') = -1742(D')^7 + 6602(D')^6 - 10174(D')^5 + 8192(D')^4 - 3679(D')^3 + 906(D')^2 - 110D' + u_{d,o} \tag{10}$$

where $u_{d,o}$ is the initial droplet velocity which for cough is 5, 10 and 15 m/s and for sneeze is 15, 20, and 25 m/s as used in the current simulations. These can simply be substituted into Equations (9) and (10) to obtain the velocity distribution with distance from the source. Droplet transport is known to be well represented by the Weber number [56]–[58]. We therefore write the one-dimensional exponential decay and growth models as a function of the weber number and the non-dimensional distance from the source follows:

$$\varphi'(D') = \begin{cases} \varphi_o + A_1 e^{-k_1 D' We_1^{b_1}} \; for \; 0 \le D' \le 0.48 \\ \varphi_o + A_2 e^{k_2 D' We_2^{b_2}} \; for \; 0.48 < D' \le 1 \end{cases} \tag{11}$$

where the asymptote φ_o represents the lowest droplet flux across the room (they are 3×10^{-8} and 1×10^{-5} for the no mask and masked cases respectively, obtained from the data as the minima at occurring at D' = 0.48); k_1 and k_2 are the decay and growth constants found by fitting the data using nonlinear least squares regression; A_1 and A_2 are the pre-exponentials also found by regression; b_1 and b_2 are fitting indices for the Weber number also obtained by the fitting process; $D' = D_s/D_{max}$ is the non-dimensional distance from the source with D_s being the distance from source and D_{max} the maximum distance droplets were sampled which is 4.2 m from the mannequin; We is the droplet Weber number defined as:

$$We = \frac{\rho \bar{u}_d^2 \bar{D}_d(D')}{\sigma} \quad (12)$$

where $\bar{u}_d$ is the mean droplet velocity at distance D' from the mannequin defined in Equations (9) and (10); while $\bar{D}_d$ is the mean droplet diameter at non-dimensional distance D' from the mannequin. The mean droplet diameter $\bar{D}_d$ is a strong function of distance from the source, i.e., $\bar{D}_d = f(D')$ and the cough and sneeze data with and without mask, it was found that 8th and 6th order polynomials very much represent this relationship. The coefficients of the polynomials depending on the case are given in Table 4 which shows that the cough cases for both with and without mask scenarios are well described by an 8th degree polynomial while the cough cases by 6th degree polynomials.

Table 4: Polynomial fit of mean sampled droplet sizes as a function of distance from source

	Coefficients of $(D')^x$										Eqn.
	$(D')^8$	$(D')^7$	$(D')^6$	$(D')^5$	$(D')^4$	$(D')^3$	$(D')^2$	(D')	$(D')^0$	R^2	No.
					Without mask						
Cough	0.023	-0.100	0.1760	-0.168	0.094	-0.032	0.006	-6.92E-4	3.26E-5	0.9138	(13)
Sneeze			0.0003	-0.002	0.003	-0.003	0.001	-1.65E-4	1.76E-5	0.9854	(14)
					With mask						
Cough	0.024	-0.0998	0.1762	-0.1676	0.094	-0.032	0.0063	-6.92E-4	3.26E-5	0.9973	(15)
Sneeze			0.0020	-0.0067	0.009	-0.006	0.0020	-3.09E-4	1.74E-5	0.9770	(16)

After nonlinear least squares fitting with the CFD droplet fluxes at each plane, the values of the constants that make Equation (11) fit the data were obtained for the non-dimensional droplet flux φ' for the mask and without mask cases. The pre-exponentials (A_1 and A_2), growth/decay constants (k_1 and k_2), and Weber number indexes (b_1 and b_2) were obtained and are as presented in Table 5. It shows that the exponential decay rate k1 for the no mask case is greater than that with the mask. This is expected as the droplets trapped in the mask mean that there is much less droplet transfer in the room hence the higher decay rate.

Table 5: Regression constants for Equation (11)

Constant	Without mask	With mask
A_1	0.00122	0.00124
A_2	2.53×10^{-5}	1.02×10^{-8}
k_1	80.612	100
K_2	4.760	4.344
b_1	1.360	2.626
b_2	1.665	1.155

Figure 15 shows that the correlation well fits the CFD data. The general trend of the data is well predicted by the correlation especially for the sneeze data possibly due to the more uniform droplet sizes compared to the cough where there the difference between the sizes of the largest and smallest droplets is more pronounced. The correlation coefficient of 0.8053 shows a high degree of confidence in the fitting and it may be concluded that the correlation well predicts the dispersion of coughed and more so sneezed droplets that may be possibly virus laden. It can be used for quickly predicting the concentration of ejected bio-aerosols in ventilated confined spaces and can give accurate results within reasonable error when compared to high-fidelity simulations or experiments which may take longer to obtain.

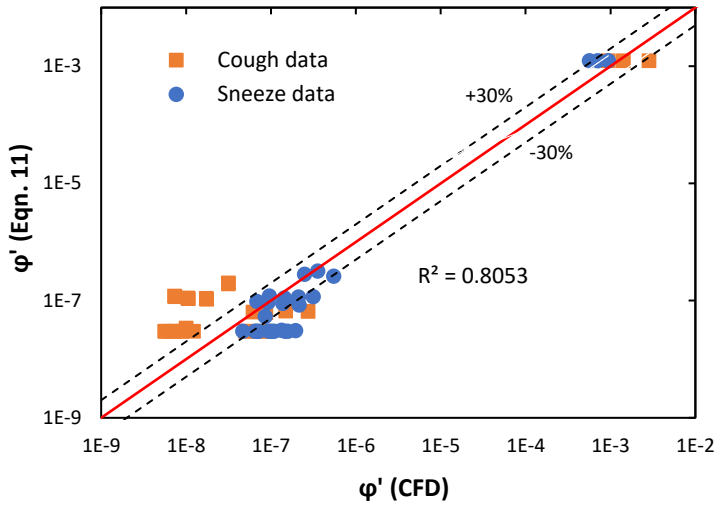

Figure 15: Correlation results of masked case droplet flux showing close agreement with CFD data

4 Conclusions

A CFD study was conducted to investigate micro-droplet transmission from a source individual to an indoor environment consisting of two connected rooms. The extent of respiratory droplet transfer from one room to the other was studied with and without a facemask. The facemask used was very porous with a 600-µm pore size. This represents the midrange of pore sizes found in typical homemade facemask fabrics, which experts have advised may be useful in preventing the transmission of infected respiratory droplets. Velocities of droplet ejecta used as boundary conditions in the simulations were obtained from experimental studies in the literature. The velocities ranged from 5 to 15 m/s and 10 to 20 m/s for coughs and sneezes, respectively. Furthermore, droplet size ranges used are between 1 to 2000 µm with a mean size of 32.6 and 17.5 µm for coughs and sneezes, respectively. Using the DPM technique, ejected droplet trajectories were studied for ejection cases with and without a facemask. The results show that the facemask trapped a vast majority of droplets. More than 90% of all droplets in both coughing and sneezing scenarios were collected in the facemask. A further 6-7% were deposited in the recommended 2 m radius social distancing area around the human, which was modelled using mannequin placed at a far corner in the source room at an oblique angle. Conversely, between 20–40% of droplets were transported between the rooms when no facemask was used. Sampled droplets deposited on the floor around the mannequin and at the door show that dispersion of droplets is greatly affected by droplet size as the smallest droplets dominate those that are transported further afield. The droplet dispersion was correlated to derive a one-dimensional exponential relationship as a function of the Weber number and distance from the source for the mask and no mask cases. In conclusion, the findings of the study reinforce the importance of using face coverings to reduce the transmission of respiratory droplets from possibly infected individuals that could transmit highly infectious coronaviruses such as the SARS CoV2 virus which causes COVID-19.

CRediT authorship contribution statement

Aliyu M. Aliyu: Conceptualisation, funding acquisition, software, writing – original draft, writing – review & editing, data curation, visualisation; Dharminder Singh: funding acquisition, software, writing – review & editing; Chino Uzoka: writing – review & editing; Rakesh Mishra: funding acquisition, supervision, writing – review & editing.

Declaration of competing interest

The authors declare that there is no known competing financial interests or personal relationships that could have appeared to influence the work reported in this paper.

Acknowledgement

The authors acknowledge the funding provided by the University of Huddersfield via the UK's Higher Education Innovation Fund (HEIF).

References

[1] WHO, "Modes of transmission of virus causing COVID-19: implications for IPC precaution recommendations," 2020. https://www.who.int/news-room/commentaries/detail/modes-of-transmission-of-virus-causing-covid-19-implications-for-ipc-precaution-recommendations (accessed May 30, 2020).

[2] K. O'reilly, J. Edmunds, A. Bennet, J. Reid, P. Horby, and C. Noakes, "Seasonality and its impact on COVID-19," 2020. Accessed: May 27, 2021. [Online]. Available: https://assets.publishing.service.gov.uk/government/uploads/system/uploads/attachment_data/file/933226/S0825_NERVTAG-EMG_Seasonality_and_its_impact_on_COVID-19.pdf.

[3] M. Lipsitch, "Seasonality of SARS-CoV-2: Will COVID-19 go away on its own in warmer weather? ," *Harvard School of Public Health – Center for Communicable Disease Dynamics*, 2020. https://ccdd.hsph.harvard.edu/will-covid-19-go-away-on-its-own-in-warmer-weather/ (accessed May 27, 2021).

[4] G. Correia, L. Rodrigues, M. Gameiro da Silva, and T. Gonçalves, "Airborne route and bad use of ventilation systems as non-negligible factors in SARS-CoV-2 transmission," *Medical Hypotheses*, vol. 141, p. 109781, 2020, doi: https://doi.org/10.1016/j.mehy.2020.109781.

[5] H. Nishimura, S. Sakata, and A. Kaga, "A new methodology for studying dynamics of aerosol particles in sneeze and cough using a digital high-vision, high-speed video system and vector analyses," *PLoS ONE*, vol. 8, no. 11, 2013, doi: 10.1371/journal.pone.0080244.

[6] Ansys, "Facing COVID-19 Challenges With Our Customers and Partners," 2020. https://www.ansys.com/about-ansys/covid-19-simulation-insights (accessed Apr. 21, 2020).

[7] Guillermo Giraldo, "How To Use CFD To Simulate Airflow in an Operating Room," *SIMSCALE Blog*, 2019. https://www.simscale.com/blog/2018/12/cfd-airflow-operating-room/ (accessed May 30, 2020).

[8] Ansys, "What a difference social distancing makes," Canonsburg, PA, USA, 2020.

[9] B. Blocken, F. Malizia, T. van Druenen, and T. Marchal, "Towards aerodynamically equivalent COVID19 1.5 m social distancing for walking and running," *Urban Physics*, p. 11, 2020.

[10] J. Couch, "Engineering professor contributes to research on containment of COVID-19 in hospitals nationwide," *Liberty News*, 2020. https://www.liberty.edu/news/index.cfm?PID=18495&MID=379373 (accessed Apr. 22, 2020).

[11] S. W. X. Ong *et al.*, "Air, Surface Environmental, and Personal Protective Equipment Contamination by Severe Acute Respiratory Syndrome Coronavirus 2 (SARS-CoV-2) from a Symptomatic Patient," *JAMA - Journal of the American Medical Association*, vol. 323, no. 16, pp. 1610–1612, 2020, doi: 10.1001/jama.2020.3227.

[12] L. Bourouiba, “Turbulent Gas Clouds and Respiratory Pathogen Emissions: Potential Implications for Reducing Transmission of COVID-19,” *JAMA - Journal of the American Medical Association*, vol. 323, no. 18, pp. 1837–1838, 2020, doi: 10.1001/jama.2020.4756.

[13] M. van der Sande, P. Teunis, and R. Sabel, “Professional and home-made face masks reduce exposure to respiratory infections among the general population,” *PLoS ONE*, vol. 3, no. 7, pp. 3–8, 2008, doi: 10.1371/journal.pone.0002618.

[14] Scientists, “Scientists join calls for UK public to wear homemade face masks outdoors,” *The Guardian*, Apr. 21, 2020.

[15] Q. X. Ma, H. Shan, H. L. Zhang, G. M. Li, R. M. Yang, and J. M. Chen, “Potential utilities of mask-wearing and instant hand hygiene for fighting SARS-CoV-2,” *Journal of Medical Virology*, no. March, pp. 1567–1571, 2020, doi: 10.1002/jmv.25805.

[16] CDC, “Recommendation Regarding the Use of Cloth Face Coverings, Especially in Areas of Significant Community-Based Transmission,” *Centers for Disease Control and Prevention - Coronavirus Disease 2019 (COVID-19)*, 2020. https://www.cdc.gov/coronavirus/2019-ncov/prevent-getting-sick/cloth-face-cover.html (accessed Apr. 22, 2020).

[17] CDC, “How to Make Your Own Face Covering,” 2020. https://www.youtube.com/watch?v=tPx1yqvJgf4 (accessed Aug. 19, 2020).

[18] Healthline, “Can Face Masks Protect You from the 2019 Coronavirus? What Types, When and How to Use,” *Healthline*, 2020. https://www.healthline.com/health/coronavirus-mask#protection (accessed Apr. 22, 2020).

[19] O. Aydin, M. A. B. Emon, S. Cheng, L. Hong, L. Chamorro, and M. T. A. Saif, “Performance of Fabrics for Home-Made Masks Against the Spread of Respiratory Infections Through Droplets: A Quantitative Mechanistic Study,” pp. 1–26, 2020, doi: 10.1101/2020.04.19.20071779.

[20] N. H. L. Leung *et al.*, “Respiratory virus shedding in exhaled breath and efficacy of face masks,” *Nature Medicine*, vol. 26, no. 5, pp. 676–680, May 2020, doi: 10.1038/s41591-020-0843-2.

[21] S. Esposito, N. Principi, C. C. Leung, and G. B. Migliori, “Universal use of face masks for success against COVID-19: evidence and implications for prevention policies,” *European Respiratory Journal*, vol. 55, no. 6, p. 2001260, Jun. 2020, doi: 10.1183/13993003.01260-2020.

[22] J. Howard *et al.*, “Face Mask Against COVID-19: An Evidence Review,” *British Medical Journal*, no. April, pp. 1–8, 2020, doi: 10.20944/preprints202004.0203.v1.

[23] S. Rossettie, C. Perry, M. Pourghaed, and M. Zumwalt, “Effectiveness of manufactured surgical masks, respirators, and home-made masks in prevention of respiratory infection due to airborne microorganisms,” *The Southwest Respiratory and Critical Care Chronicles*, vol. 8, no. 34, pp. 11–26, Apr. 2020, doi: 10.12746/swrccc.v8i34.675.

[24] P. Kalliomäki, P. Saarinen, J. W. Tang, and H. Koskela, “Airflow Patterns through Single Hinged and Sliding Doors in Hospital Isolation Rooms,” *International Journal of Ventilation*, vol. 14, no. 2, pp. 111–126, Sep. 2015, doi: 10.1080/14733315.2015.11684074.

[25] P. E. Saarinen, P. Kalliomäki, J. W. Tang, and H. Koskela, “Large Eddy Simulation of Air Escape through a Hospital Isolation Room Single Hinged Doorway—Validation by Using Tracer Gases and Simulated Smoke Videos,” *PLOS ONE*, vol. 10, no. 7, p. e0130667, Jul. 2015, doi: 10.1371/journal.pone.0130667.

[26] J. W. Tang *et al.*, "Different Types of Door-Opening Motions as Contributing Factors to Containment Failures in Hospital Isolation Rooms," *PLOS ONE*, vol. 8, no. 6, p. e66663, Jun. 2013.

[27] P. Kalliomäki, P. Saarinen, J. W. Tang, and H. Koskela, "Airflow patterns through single hinged and sliding doors in hospital isolation rooms – Effect of ventilation, flow differential and passage," *Building and Environment*, vol. 107, pp. 154–168, 2016, doi: 10.1016/j.buildenv.2016.07.009.

[28] H. Qian and Y. Li, "Removal of exhaled particles by ventilation and deposition in a multibed airborne infection isolation room," *Indoor Air*, vol. 20, no. 4, pp. 284–297, Mar. 2010, doi: 10.1111/j.1600-0668.2010.00653.x.

[29] ASHRAE, "Standard methods for laboratory air-flow measurement. American Society of Heating, Refrigerating and Air-Conditioning Engineers." Atlanta, p. Standard 41.2-1987, 1987.

[30] FGI, "Guidelines for Design and Construction of Hospitals and Outpatient Facilities." Facilities Guidelines Institute Dallas, TX, 2014.

[31] A. Ragab, A. Fouda, H. El-Deeb, and H. Abou-Taleb, "Determination of Pore Size, Porosity and Pore Size Distribution of Woven Structures by Image Analysis Techniques," *Journal of Textile Science & Engineering*, vol. 07, no. 05, 2017, doi: 10.4172/2165-8064.1000314.

[32] T. Asim, R. Mishra, A. Oliveira, and M. Charlton, "Effects of the geometrical features of flow paths on the flow capacity of a control valve trim," *Journal of Petroleum Science and Engineering*, vol. 172, pp. 124–138, Jan. 2019, doi: 10.1016/J.PETROL.2018.09.050.

[33] M. O. Altwieb and R. Mishra, "Experimental and Numerical Investigations on the Response of a Multi Tubes and Fins Heat Exchanger under Steady State Operating Conditions Original Citation the Response of a Multi Tubes and Fins Heat Exchanger under," in *6th International and 43rd National Conference on Fluid Mechanics and Fluid Power*, 2016, pp. 1–3.

[34] T. Asim, A. Oliveira, M. Charlton, and R. Mishra, "Improved design of a multi-stage continuous-resistance trim for minimum energy loss in control valves," *Energy*, vol. 174, pp. 954–971, May 2019, doi: 10.1016/j.energy.2019.03.041.

[35] A. M. Aliyu, Y. K. Kim, S. H. Choi, J. H. Ahn, and K. C. Kim, "Development of a dual optical fiber probe for the hydrodynamic investigation of a horizontal annular drive gas/liquid ejector," *Flow Measurement and Instrumentation*, vol. 56, pp. 45–55, Aug. 2017, doi: 10.1016/j.flowmeasinst.2017.07.005.

[36] D. Singh, A. M. Aliyu, M. Charlton, R. Mishra, T. Asim, and A. Oliveira, "Local multiphase flow characteristics of a severe-service control valve," *Journal of Petroleum Science and Engineering*, 2020.

[37] J. Hang, Z. Luo, M. Sandberg, and J. Gong, "Natural ventilation assessment in typical open and semi-open urban environments under various wind directions," *Building and Environment*, vol. 70, pp. 318–333, Dec. 2013, doi: 10.1016/j.buildenv.2013.09.002.

[38] S. Hussain, P. H. Oosthuizen, and A. Kalendar, "Evaluation of various turbulence models for the prediction of the airflow and temperature distributions in atria," *Energy and Buildings*, vol. 48, pp. 18–28, May 2012, doi: 10.1016/j.enbuild.2012.01.004.

[39] C. Heschl, K. Inthavong, W. Sanz, and J. Tu, “Evaluation and improvements of RANS turbulence models for linear diffuser flows,” *Computers and Fluids*, vol. 71, pp. 272–282, Jan. 2013, doi: 10.1016/j.compfluid.2012.10.015.

[40] S. A. Morsi and A. J. Alexander, “An investigation of particle trajectories in two-phase flow systems,” *Journal of Fluid Mechanics*, vol. 55, no. 2, pp. 193–208, 1972, doi: 10.1017/S0022112072001806.

[41] Ansys, “Equation of Motion for Particles,” *User Guide*, 2009. https://www.afs.enea.it/project/neptunius/docs/fluent/html/th/node241.htm (accessed Aug. 16, 2020).

[42] T. Asim, R. Mishra, S. Abushaala, and A. Jain, “Development of a design methodology for hydraulic pipelines carrying rectangular capsules,” *International Journal of Pressure Vessels and Piping*, vol. 146, pp. 111–128, Oct. 2016, doi: 10.1016/j.ijpvp.2016.07.007.

[43] T. Asim and R. Mishra, “Optimal design of hydraulic capsule pipelines transporting spherical capsules,” *The Canadian Journal of Chemical Engineering*, vol. 94, no. 5, pp. 966–979, May 2016, doi: 10.1002/cjce.22450.

[44] J. W. Tang *et al.*, “Airflow Dynamics of Human Jets: Sneezing and Breathing - Potential Sources of Infectious Aerosols,” *PLoS ONE*, vol. 8, no. 4, pp. 1–7, 2013, doi: 10.1371/journal.pone.0059970.

[45] S. B. Kwon *et al.*, “Study on the initial velocity distribution of exhaled air from coughing and speaking,” *Chemosphere*, vol. 87, no. 11, pp. 1260–1264, 2012, doi: 10.1016/j.chemosphere.2012.01.032.

[46] C. Y. H. Chao *et al.*, “Characterization of expiration air jets and droplet size distributions immediately at the mouth opening,” *Journal of Aerosol Science*, vol. 40, no. 2, pp. 122–133, 2009, doi: 10.1016/j.jaerosci.2008.10.003.

[47] B. E. Scharfman, A. H. Techet, J. W. M. Bush, and L. Bourouiba, “Visualization of sneeze ejecta: steps of fluid fragmentation leading to respiratory droplets,” *Experiments in Fluids*, vol. 57, no. 2, p. 24, Feb. 2016, doi: 10.1007/s00348-015-2078-4.

[48] T. Dbouk and D. Drikakis, “On coughing and airborne droplet transmission to humans,” *Physics of Fluids*, vol. 32, no. 5, p. 053310, 2020, doi: 10.1063/5.0011960.

[49] L. Bourouiba, E. Dehandschoewercker, and J. W. M. Bush, “Violent expiratory events: on coughing and sneezing,” *Journal of Fluid Mechanics*, vol. 745, pp. 537–563, Apr. 2014, doi: 10.1017/jfm.2014.88.

[50] X. Xie, Y. Li, H. Sun, and L. Liu, “Exhaled droplets due to talking and coughing,” *Journal of the Royal Society Interface*, vol. 6, no. SUPPL. 6, 2009, doi: 10.1098/rsif.2009.0388.focus.

[51] S. Ward-smith, “Droplet sizing of coughs and sneezes,” 2020. https://www.materials-talks.com/blog/2020/04/15/droplet-sizing-of-coughs-and-sneezes/ (accessed Jul. 03, 2020).

[52] Z. Y. Han, W. G. Weng, and Q. Y. Huang, “Characterizations of particle size distribution of the droplets exhaled by sneeze,” *Journal of the Royal Society Interface*, vol. 10, no. 88, 2013, doi: 10.1098/rsif.2013.0560.

[53] J. P. Duguid, “The size and the duration of air-carriage of respiratory droplets and droplet-nuclei,” *Journal of Hygiene*, vol. 44, no. 6, pp. 471–479, 1946, doi: 10.1017/S0022172400019288.

[54] J. Wei and Y. Li, “Human cough as a two-stage jet and its role in particle transport,” *PLoS ONE*, vol. 12, no. 1, pp. 1–15, 2017, doi: 10.1371/journal.pone.0169235.

[55] S. Leonard, L. Volakis, R. DeBellis, A. Kahlon, and S. Mayar, “TRANSMISSION ASSESSMENT REPORT: High Velocity Nasal Insufflation (HVNI) Therapy Application in Management of COVID-19,” 2020.

[56] A. M. Aliyu *et al.*, “Prediction of entrained droplet fraction in co-current annular gas–liquid flow in vertical pipes,” *Experimental Thermal and Fluid Science*, vol. 85, pp. 287–304, Jul. 2017, doi: 10.1016/j.expthermflusci.2017.03.012.

[57] J. R. Barbosa, G. F. Hewitt, G. König, and S. M. Richardson, “Liquid entrainment, droplet concentration and pressure gradient at the onset of annular flow in a vertical pipe,” *International Journal of Multiphase Flow*, vol. 28, no. 6, pp. 943–961, 2002, doi: 10.1016/S0301-9322(02)00003-4.

[58] Y. Xu, A. M. Aliyu, H. Seo, J. J. Wang, and K. C. Kim, “Effect of crossflow velocity on underwater bubble swarms,” *International Journal of Multiphase Flow*, vol. 105, pp. 60–73, 2018, doi: 10.1016/j.ijmultiphaseflow.2018.03.018.

Appendix: Close up figures of facemask mesh and droplet cone injection

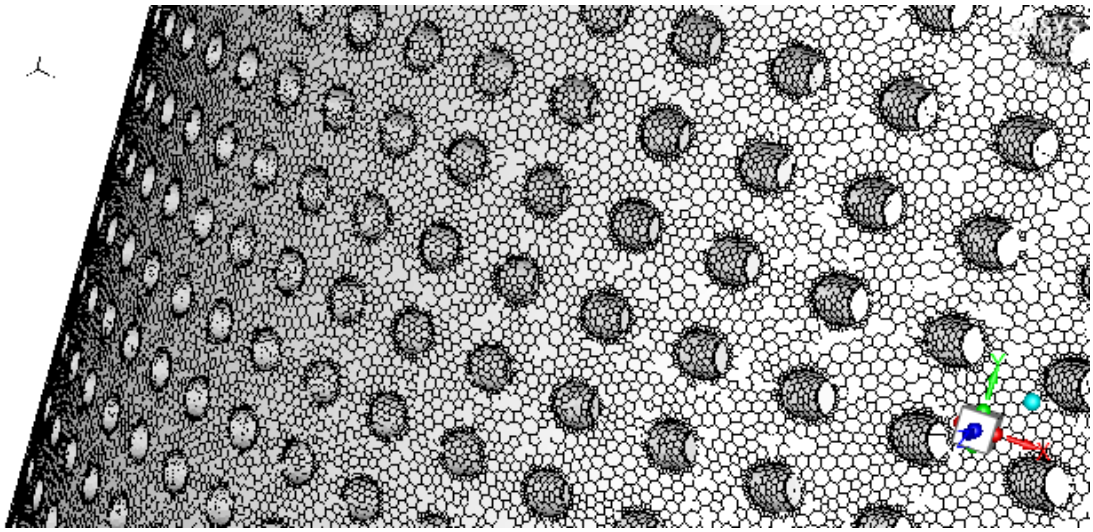

Figure A1: Surface of mask with polyhedral mesh element imprints showing their relative size in comparison to the holes.

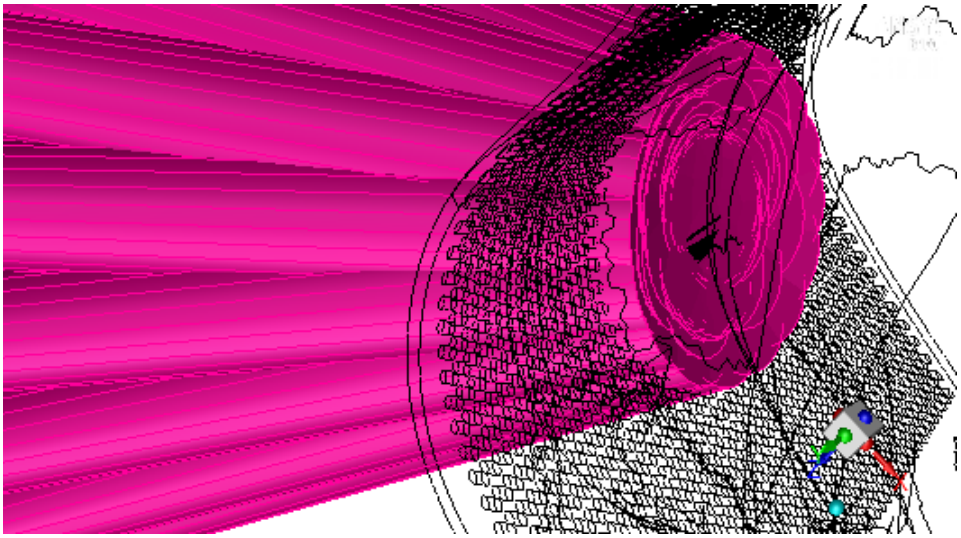

Figure A2: Depiction of cone injection between face mask and mannequin's face.